



Deposited via The University of Sheffield.

White Rose Research Online URL for this paper:

<https://eprints.whiterose.ac.uk/id/eprint/154996/>

Version: Accepted Version

Article:

Galindo-Trigo, S., Blanco-Touriñán, N., DeFalco, T.A. et al. (2020) CrRLK1L receptor-like kinases HERK1 and ANJEA are female determinants of pollen tube reception. *EMBO Reports*, 21 (2). e48466. ISSN: 1469-221X

<https://doi.org/10.15252/embr.201948466>

© 2019 The Authors. This is an author-produced version of a paper subsequently published in *EMBO Reports*. Uploaded in accordance with the publisher's self-archiving policy.

Reuse

Items deposited in White Rose Research Online are protected by copyright, with all rights reserved unless indicated otherwise. They may be downloaded and/or printed for private study, or other acts as permitted by national copyright laws. The publisher or other rights holders may allow further reproduction and re-use of the full text version. This is indicated by the licence information on the White Rose Research Online record for the item.

Takedown

If you consider content in White Rose Research Online to be in breach of UK law, please notify us by emailing eprints@whiterose.ac.uk including the URL of the record and the reason for the withdrawal request.

1 **CrRLK1L receptor-like kinases HERCULES RECEPTOR**
2 **KINASE 1 and ANJEA are female determinants of pollen tube**
3 **reception**

4
5 Sergio Galindo-Trigo^{1,2}, Noel Blanco-Touriñán³, Thomas A. DeFalco^{4,5}, Eloise S. Wells¹, Julie E
6 Gray⁶, Cyril Zipfel^{4,5}, Lisa M Smith^{1*}

7
8 ¹Department of Animal and Plant Sciences, University of Sheffield, Western Bank, Sheffield S10
9 2TN, UK

10
11 ²Department of Biosciences, University of Oslo, P.O. Box 1066 Blindern
12 0316 Oslo, Norway

13
14 ³Instituto de Biología Molecular y Celular de Plantas, Consejo Superior de Investigaciones
15 Científicas, Universidad Politécnica de Valencia, Valencia, Spain

16
17 ⁴The Sainsbury Laboratory, University of East Anglia, Norwich Research Park, Norwich NR4 7UH,
18 UK

19
20 ⁵Department of Molecular and Cellular Plant Physiology and Zurich-Basel Plant Science Center,
21 University of Zurich, Zollikerstrasse 107, CH-8008 Zurich, Switzerland

22
23 ⁶Department of Molecular Biology and Biotechnology, University of Sheffield, Western Bank,
24 Sheffield S10 2TN, UK

25
26
27 *Corresponding author: lisa.m.smith@sheffield.ac.uk
28
29
30
31
32
33

34 **Running title:** HERK1 and ANJ regulate fertilisation
35
36
37
38
39
40
41
42

43 **Abstract**

44 Communication between the gametophytes is vital for angiosperm fertilisation. Multiple *CrRLK1L*-
45 type receptor kinases prevent premature pollen tube burst, while another *CrRLK1L* protein,
46 FERONIA (FER), is required for pollen tube reception in the female gametophyte. We report here
47 the identification of two additional *CrRLK1L* homologues, HERCULES RECEPTOR KINASE 1
48 (HERK1) and ANJEA (ANJ), which act redundantly to promote pollen tube growth arrest at the
49 synergid cells. HERK1 and ANJ localise to the filiform apparatus of the synergid cells in unfertilised
50 ovules, and in *herk1 anj* mutants a majority of ovules remain unfertilised due to pollen tube
51 overgrowth, together indicating that HERK1 and ANJ act as female determinants for fertilisation.
52 As in *fer* mutants, the synergid cell-specific, endomembrane protein NORTIA (NTA) is not
53 relocalised after pollen tube reception; however, unlike *fer* mutants, reactive oxygen species levels
54 are unaffected in *herk1 anj* double mutants. Both ANJ and HERK1 associate with FER and its
55 proposed co-receptor LORELEI (LRE) *in planta*. Together, our data indicate that HERK1 and ANJ
56 act with FER to mediate female-male gametophyte interactions during plant fertilisation.

57

58 **Keywords**

59 *CrRLK1L*, Fertilisation, Synergid cells, Receptor kinase, Angiosperm

60

61

62 **Short summary of findings**

63 The *CrRLK1L* receptor kinases HERK1 and ANJ are genetically redundant during pollen
64 tube reception in Arabidopsis. Both proteins interact with the *CrRLK1L* receptor FER and
65 its putative co-receptor LRE, however the role of FER in fertilisation extends to production
66 of reactive oxygen species in ovules while HERK1 and ANJ are not involved in this
67 process.

68

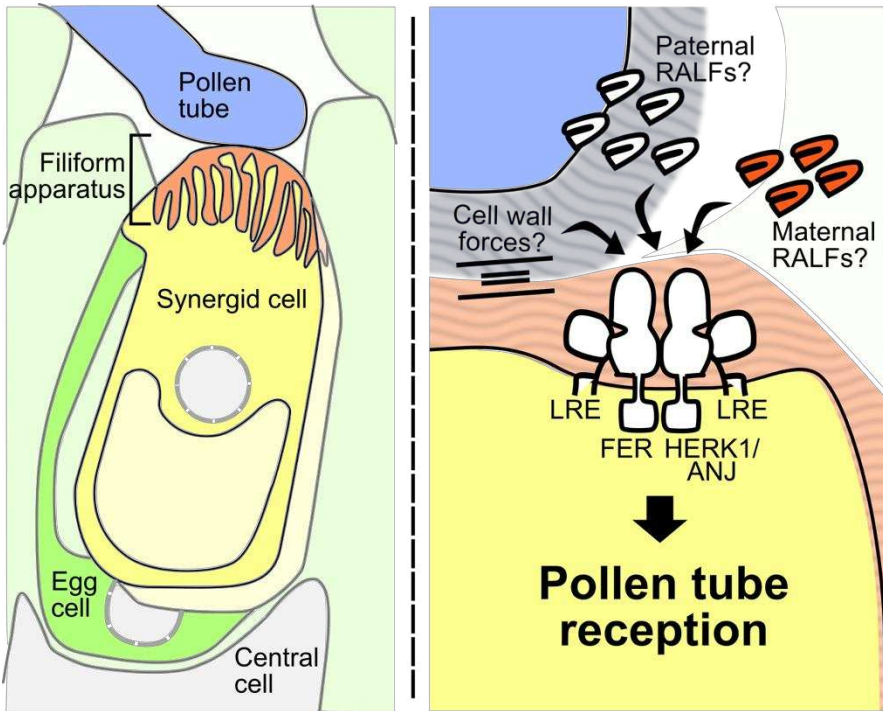
69 **Key results**

- 70 • Double mutants of HERK1 and ANJ produce fewer seeds as pollen tube overgrowth
71 occurs in the majority of ovules in a maternally-controlled phenotype.
- 72 • HERK1 and ANJ are both expressed in the synergid cells, where other fertilisation
73 components in the form of *CrRLK1L* receptor FERONIA, its co-receptor LORELEI,
74 and downstream protein NORTIA are also located.
- 75 • Kinase activity of HERK1 and ANJ is not required for complementation of the pollen
76 tube reception phenotype.
- 77 • HERK1 and ANJ interact with FER and LRE.
- 78 • Unlike FER, HERK1 and ANJ are not required for pre-fertilisation production of
79 reactive oxygen species.

80

81

82 **Synopsis picture**



83

84

85 **Introduction**

86 Fertilisation is a critical point in the life cycle of any sexually reproducing organism. In flowering
87 plants, gametes are enclosed in gametophytes, multicellular structures that develop in the
88 reproductive organs of the flower. The pollen grain constitutes the male gametophyte, with each
89 grain generating a pollen tube in the form of a rapidly growing cellular protrusion that delivers the
90 male gametes, or sperm cells, through the style tissues into the ovule. Female gametophytes
91 develop inside the ovule and contain the female gametes within an embryo sac; the egg cell and
92 central cell. The process of double fertilisation in angiosperms consists of the fusion of a sperm cell
93 with each of the female gametes. If fertilisation is successful, the embryo and endosperm develop
94 from the egg cell and central cell fertilisations, respectively. For double fertilisation to occur, the
95 male and female gametophytes must engage in a molecular dialog that controls pollen tube
96 attraction towards the ovule entrance, or micropyle, the arrest of pollen tube growth and the
97 release of the sperm cells in the correct location within the ovule (see [1,2] for a detailed review).

98 The synergid cells occupy the micropylar portion of the female gametophyte, and aid
99 communication between the gametophytes. As such, their cytoplasm is densely occupied by
100 endomembrane compartments, reflective of a highly active secretion system generating
101 messenger molecules [3]. The filiform apparatus appears at the outermost pole, a thickened and
102 intricate cell wall structure that represents the first contact point between female and male
103 gametophytes prior to fertilisation [4]. Synergid cells secrete small cysteine-rich LURE and XIUQIU
104 peptides to guide pollen tubes towards the embryo sac [5,6]. AtLURE1 peptides are sensed by two
105 pairs of pollen-specific receptor-like kinases (RLKs), MALE DISCOVERER 1 (MDIS1) and MDIS1-
106 INTERACTING RLK 1 (MIK1), and POLLEN-SPECIFIC RECEPTOR KINASE 6 (PRK6) and PRK3
107 in Arabidopsis [7,8]. These RLKs bind AtLURE1 peptides through their extracellular domains at the
108 growing tip of the pollen tubes, promoting their exit from the transmitting tract in a species-specific
109 manner [6-9]. XIUQIU peptides, on the other hand, attract pollen tubes towards the synergid cells
110 regardless of the species, and signalling through a pollen tube receptor is yet to be described [6].

111 Within the expanded family of RLKs in Arabidopsis, the *Catharanthus roseus* RLK1-like (*CrRLK1L*)
112 subfamily has been demonstrated to play several roles during fertilisation (see [10] for a detailed
113 review). Two pairs of functionally redundant *CrRLK1L*s are integral in controlling pollen tip growth,
114 ANXUR1 and 2 (ANX1/2), and BUDDHA'S PAPER SEAL 1 and 2 (BUPS1/2), heterodimerise and
115 ensure pollen tube growth by sensing of two autocrine secreted peptides belonging to the RAPID
116 ALKALINIZATION FACTOR (RALF) family, RALF4 and RALF19 [11-14]. A fifth *CrRLK1L* protein,
117 ERULUS (ERU), has also been implicated in male-determined pollen tube growth via regulation of
118 Ca²⁺ oscillations [15]. The *CrRLK1L* protein FERONIA (FER) accumulates in the filiform apparatus
119 of the synergids where it functions as a female determinant of pollen tube reception and
120 subsequent sperm cell release [16,17]. Although no extracellular ligand has been identified for
121 FER in a reproductive context, there is evidence for FER activation of a synergid-specific signalling
122 cascade upon pollen tube arrival. This signalling pathway involves the glycosyl-phosphatidylinositol
123 (GPI)-anchored protein LORELEI (LRE) [18,19], activation of NADPH oxidases to generate
124 reactive oxygen species (ROS) in the micropyle [20], generation of specific Ca²⁺ signatures in the
125 synergid cytoplasm [21], and relocalisation of the Mildew resistance locus O (MLO)-like NORTIA
126 (NTA), an endomembrane compartment protein that affects pollen tube-induced Ca²⁺ signatures in
127 the synergids [21-23].

128 *CrRLK1L* receptor kinases have also been assigned a number of other functions beyond
129 fertilisation. For example, cell elongation during vegetative growth requires several members of the
130 *CrRLK1L* family; HERCULES RECEPTOR KINASES 1 and 2 (HERK1 and 2), THESEUS1 (THE1)
131 and FER [24,25]. FER has also been linked to pathogen responses [26], while THE1 and other
132 *CrRLK1L* receptors detect cell wall integrity [27].

133 Many questions remain about the nature of the communication between gametophytes that
134 controls sperm cell release, and *CrRLK1L*s FER, ANX1/2 and BUPS1/2 are potential receptor
135 candidates to mediate this dialog. Here we report the characterisation of *CrRLK1L*s HERCULES
136 RECEPTOR KINASE 1 (HERK1) and ANJEA (AT5G59700; ANJ) as female determinants of pollen
137 tube reception in Arabidopsis. We show that HERK1 and ANJ act redundantly at the filiform
138 apparatus of the synergids to control pollen tube growth arrest, representing two new mediators of

139 gametophytic communication and therefore expanding the female-specific toolbox required for
140 fertilisation.

141 **Results**

142 **HERK1 and ANJ function redundantly in seed set**

143 To test whether additional Arabidopsis *CrRLK1L* proteins are involved in reproduction, we obtained
144 T-DNA insertion lines for all seventeen family members. Presence of a homozygous insertion was
145 verified for ten *CrRLK1L* genes. These verified lines were crossed and double homozygous plants
146 selected in the F2 generation by PCR genotyping (Figure EV1A-B for T-DNA lines used further in
147 this study). Stable double homozygous lines were qualitatively examined for fertility. Through this
148 screen, we identified that double mutants in *HERCULES RECEPTOR KINASE 1 (HERK1)* and
149 *AT5G59700* (hereafter referred to as *ANJEA/ANJ*) have high rates of unfertilised ovules or seeds
150 that abort very early in development, and shorter siliques (Figure 1A). The qualitative nature of our
151 preliminary screen for fertility defects in *CrRLK1L* mutants does not preclude the involvement of
152 additional *CrRLK1L*s in reproduction as quantitative investigation may uncover more subtle fertility
153 defects among the mutants of this family of receptors. HERK1 and ANJEA are close homologues
154 within the *CrRLK1L* family [28], with 75% identity and 86% similarity at the amino acid level. Loss
155 of *ANJ* gene expression in the double homozygous *herk1-1 anj-1* T-DNA line (hereafter referred to
156 as *herk1 anj*) was confirmed by RT-qPCR (Figure EV1C). Although the *herk1-1* T-DNA insertion
157 has previously been reported to knockout gene expression [24], our RT-qPCR results indicate that
158 transcripts are present at wild-type levels 5' of the T-DNA insertion, and at ~20% of wild-type levels
159 3' of the T-DNA insertion. Whether these transcripts are translated into truncated proteins would
160 require generation of α HERK1 antibodies. However, as the *herk1-1 anj-1* phenotype can be
161 complemented by expression of HERK1 and the *herk1-1 anj-1* phenotype is equivalent to other
162 mutants in the pathway (see below), we conclude that *herk1-1* likely does not act as a dominant
163 negative or hypermorphic allele within a reproductive context.

164 To verify that the low rate of seed set results from functional redundancy between *HERK1* and
165 *ANJ*, we examined seed development in dissected siliques of wild-type, *herk1*, *anj* and *herk1 anj*
166 plants grown in parallel. While single mutants *herk1* and *anj* did not have elevated numbers of
167 unfertilised/aborted seeds compared to wild-type, a high proportion of ovules in *herk1 anj* siliques
168 had not developed into mature seeds, leading to a reduced number of seeds per silique (Figure
169 1B). We therefore concluded that there is functional redundancy between the *HERK1* and *ANJ*
170 proteins during fertilisation or early seed development.

171 *HERK1* has previously been described to influence cell elongation in vegetative tissues with *THE1*
172 and *HERK2*, with the *herk1 the1-4* and *herk1 herk2 the1-4* mutants displaying a short petiole
173 phenotype, similarly to *fer* mutants [24,25]. We further examined the *herk1 anj* mutants for
174 developmental defects in vegetative and reproductive growth, finding no other developmental
175 aberrations (Appendix Figure S1). Thus, *HERK1* and *ANJ* do not act redundantly during vegetative
176 growth.

177 ***HERK1* and *ANJ* are female determinants of pollen tube reception**

178 Previous studies of *CrRLK1L* proteins where mutation results in low or absent seed set have
179 identified functions in pollen tube growth (*ANX1*, *ANX2*, *BUPS1*, *BUPS2* and *ERU*; [11-15]) and
180 female-mediated pollen tube growth arrest at the synergids (*FER* [17]). To test which step in
181 fertilisation is impaired in the *herk1 anj* mutant, we tracked pollen tube growth through the style
182 and ovary in single and double mutants. In all plant lines, aniline blue staining revealed that the
183 pollen tubes targeted the female gametophytes correctly (Appendix Figure S2). However, closer
184 examination of the ovules revealed pollen tube overgrowth at high frequency in *herk1 anj* mutants.
185 While pollen tube overgrowth is rare in wild-type and single mutants, 83% of pollen tubes failed to
186 burst upon entering ovules in the double mutant (Figure 1C). The 83% of ovules exhibiting pollen
187 tube overgrowth is notably higher than the 71% of ovules that fail to develop into seeds (Figure
188 1B,C), indicating that in some cases fertilisation occurs in the presence of pollen tube overgrowth.

189 In *fer* mutants, pollen tube overgrowth occurs due to maternal defects in male-female gametophyte
190 communications [16,17,20]. To confirm that *HERK1* and *ANJ* are female determinants of pollen
191 tube reception, we performed reciprocal crosses between the *herk1 anj* mutant and wild-type
192 plants, as well as control crosses within each plant line. While wild-type Col-0 (female; f) x *herk1*
193 *anj* (male; m) crosses resulted in 1% of ovules with pollen tube overgrowth, over 90% of pollen
194 tubes exhibited overgrowth in *herk1 anj* (f) x wild-type (m) crosses, indicating that pollen tube
195 overgrowth is a maternally-derived phenotype in *herk1 anj* mutants (Figure 1D). As expected,
196 pollen tube overgrowth was observed in only 3% of the ovules in the control wild-type (f) x wild-
197 type (m) crosses, while 89% of ovules had overgrowth of the pollen tube in *herk1 anj* (f) x *herk1 anj*
198 (m) crosses.

199 To verify that the reproductive defect is due to the disruption of the *HERK1* and *ANJ* genes and
200 does not arise from additional T-DNA insertions, we reintroduced the *HERK1* and *ANJ* genes into
201 the *herk1 anj* background to test for complementation of the pollen tube overgrowth phenotype.
202 We generated *pHERK1::HERK1* and *pANJ::ANJ-GFP* constructs and found that while
203 *pHERK1::HERK1* could be generated, *pHERK1::HERK1-GFP* could not be cloned due to toxicity in
204 several bacterial strains. This could explain why a *pBRI1::HERK1-GFP* construct has previously
205 been used to complement the *herk1* mutant [24]. *FERONIA*'s promoter presents a broad
206 expression pattern in ovules [29], and given the maternal origin of the reproductive defect in *herk1*
207 *anj* plants, we decided to use *pFER::HERK1-GFP* to test for complementation. In the developing
208 ovules of five independent T1 plants where a hemizygous insertion would segregate 50:50,
209 expression of *pFER::HERK1-GFP* or *pANJ::ANJ-GFP* constructs in the *herk1 anj* background
210 reduced pollen tube overgrowth by ~50%, as did a *pHERK1::HERK1* construct (Appendix Figure
211 S3). Complementation indicates that these reporter constructs produce functional proteins and
212 confirms that the T-DNA insertions in the *HERK1* and *ANJ* genes are responsible for pollen tube
213 overgrowth. We conclude that *HERK1* and *ANJ* are female determinants of pollen tube reception
214 and therefore named *AT5G59700* after a fertility goddess in Australian aboriginal mythology,
215 Anjea.

216 The kinase activity of FER is not required for its control of pollen tube reception in ovules [29]. We
217 therefore tested for complementation of the *herk1 anj* reproductive defect with kinase-dead (KD)
218 versions of HERK1 and ANJ. HERK1-KD and ANJ-KD were generated by targeted mutagenesis of
219 key residues within the kinase activation loop (D609N/K611R for HERK1 and D606N/K608R for
220 ANJ; [30]) that render the kinase domains inactive, as demonstrated by *in vitro* phosphorylation
221 assays using recombinant HERK1(D609N/K611R) and ANJ(D606N/K608R) kinase domains
222 (Figure EV2A). *pHERK1::HERK1-KD* and *pANJ::ANJ-KD-GFP* were also able to complement the
223 pollen overgrowth phenotype, indicating that the kinase activity of these RLKs is not required for
224 their function in fertilisation (Figure EV2B). As kinase activity was not required for complementation
225 of the *herk1 anj* phenotype, we also made a *pHERK1::HERK1-KD-GFP* construct to test for
226 complementation by HERK1 when expressed under its native promoter. Seed set was confirmed
227 to be complemented to the expected extent in T1 plants (Appendix Figure S4A). The similarity in
228 the mutant phenotypes and the dispensable kinase activity in HERK1/ANJ and FER suggests they
229 may act in the same signalling pathway as co-receptors or as parallel receptor systems.

230

231 **HERK1 and ANJ are localised to the filiform apparatus**

232 To explore the localisation of HERK1 and ANJ in the female gametophyte and hence gain insight
233 into the possible function of HERK1/ANJ in fertilisation, we made *promoter::H2B-TdTomato*
234 transcriptional fusions where expression of either the *HERK1* or *ANJ* promoter should direct
235 nuclear localisation of an RFP signal. Both *HERK1* and *ANJ* were strongly expressed in
236 unfertilized embryo sacs, with expression of *HERK1* in the two synergid cells, egg cell and central
237 cell of 4-cell stage female gametophytes and *ANJ* expression restricted to the two synergid cells
238 (Figure 2A-D). As HERK1 and ANJ must be expressed in the same cells for a genetic interaction to
239 occur, this restricts their potential function in the female gametophyte during fertilisation to the
240 synergid cells.

241 We next generated *promoter::GUS* (β -glucuronidase) transcriptional fusions to gain insight into the
242 expression of these genes at a tissue level. *pHERK1::GUS* is also expressed in the style, ovary
243 walls and stamens (Appendix Figure S5A-E), whereas *pANJ::GUS* expression is detected in
244 stigmas and stamen filaments (Appendix Figure S5F-J). No expression was detected in pollen
245 grains within mature anthers, although *HERK1* was expressed in some developing pollen grains
246 (Appendix Figure S5B,D,I). Within the siliques, *HERK1* was most highly expressed close to the
247 stigma, while *ANJ* appears to be expressed in the funiculus (Appendix Figure S5E,J). Thus *HERK1*
248 and *ANJ* are expressed in multiple reproductive tissues, with the pattern of expression suggesting
249 the fertilisation defect may arise through a biological function in the junction of the stigma and
250 style, or in the female gametophyte where *HERK1* and *ANJ* gene expression overlaps in the
251 synergid cells.

252 To further examine *HERK1* and *ANJ* expression and subcellular localisation in ovules, we used the
253 *pANJ::ANJ-GFP*, *pFER::HERK1-GFP* and *pHERK1::HERK1-KD-GFP* constructs that complement
254 the fertilisation phenotype. Examination of fluorescent signals from *HERK1-GFP* and *ANJ-GFP*
255 fusion proteins in the female gametophyte showed that they were strongly localised to the filiform
256 apparatus of the synergid cells (Figure 2E-H, Appendix Figure S4B,C). The filiform apparatus is a
257 structure formed by dense folds in the plasma membrane and cell wall where the regulators of
258 fertilisation *FER* and *LRE* also localise [17,19,31]. This specific cellular localisation supports the
259 hypothesis that *HERK1* and *ANJ* could function in the same pathway as *FER* and *LRE*. While loss
260 of *FER* or *LRE* alone leads to a reproductive defect caused by pollen tube overgrowth in the ovule
261 [17,19], *HERK1* and *ANJ* are functionally redundant, such that *HERK1* and *ANJ* could act as
262 alternative co-receptors for *FER* and/or *LRE* during male-female interactions.

263 **NORTIA relocalisation after fertilisation is impaired in *herk1 anj* mutants**

264 Previous reports point to an interdependence between *FER*, *LRE* and *NTA* in their respective
265 cellular localisations [18,22]. *FER* only accumulates in the filiform apparatus if functional *LRE* is
266 present, and *NTA* relocalisation towards the filiform apparatus upon pollen tube arrival is
267 dependent on *FER* [18,22]. As *HERK1* and *ANJ* may act in the same signalling pathway as *FER*,

268 we tested the localisation of fluorescence-tagged HERK1, ANJ, FER, LRE and NTA in the *herk1*
269 *anj* and *lre-5* backgrounds (Figure 3A). Localisation within the synergids of FER-GFP, LRE-Citrine
270 and NTA-GFP was not affected by *herk1 anj* mutations. Similarly, HERK1-GFP and ANJ-GFP
271 localised to the filiform apparatus in the *lre-5* background. Contrary to previous findings [18], under
272 our conditions FER-GFP accumulation in the filiform apparatus was not impaired in *lre-5* plants
273 ($n>25$; FER-GFP was found at the filiform apparatus in all ovules checked). To verify that FER
274 subcellular localisation was not affected in *lre-5* under our growth conditions, we quantified the
275 mean fluorescence intensity across the filiform apparatus (FA) and synergid cytoplasm (SC) to
276 calculate the ratio of FA:SC fluorescence intensity (Figure EV3A). When compared across the
277 wild-type, *herk1 anj* and *lre-5* genotypes, the mean FA:SC fluorescence intensity ratios were not
278 significantly different, indicating no effect on FER-GFP localisation to the FA in plants lacking LRE
279 or HERK1/ANJ. Furthermore, we found no differences in the percentage of ovules presenting
280 moderate or severe mislocalisation of FER-GFP in the synergid cells in wild-type, *herk1 anj* or *lre-5*
281 plants (Student's *t* tests, $p>0.05$; Figure EV3B). Therefore, we found no dependency on
282 HERK1/ANJ or LRE for localisation of FER, LRE, HERK1, ANJ or NTA within the synergids of
283 unfertilised ovules.

284 To determine whether NTA relocalisation in synergid cells upon pollen tube arrival depends on
285 functional HERK1 and ANJ, we transformed *pMYB98::NTA-GFP* into the *herk1 anj* background.
286 Using SR2200-based callose staining to visualise the filiform apparatus and pollen tube, we
287 observed NTA-GFP fluorescence intensity across the length of the synergid cell. In unfertilised
288 ovules, NTA-GFP fluorescence is evenly distributed across the length of the synergid cell in wild-
289 type and *herk1 anj* plants (Figure 3B). Wild-type fertilised ovules have a shift in the fluorescence
290 intensity pattern, with NTA accumulation towards the micropylar end of the synergid cytoplasm and
291 a decrease in relative fluorescence intensity towards the chalazal end (Figure 3B-C). This
292 response is absent in *herk1 anj* fertilised ovules in which the relative fluorescence intensity pattern
293 is indistinguishable from that of unfertilised ovules, indicating a requirement for HERK1/ANJ in
294 NTA relocalisation upon pollen tube perception.

295 Whether LRE is dispensable for NTA relocalisation upon pollen tube arrival has not previously
296 been tested. We therefore transformed the *pMYB98::NTA-GFP* construct into the *lre-5* genetic
297 background and repeated the assay above to examine whether LRE is required for NTA
298 relocalisation as for *HERK1*, *ANJ* and *FER* [22]. While a region of statistically lower signal intensity
299 was present around the middle of the synergids in pollinated *lre-5* ovules compared to wild-type
300 virgin ovules (Figure 3D), there was no significant shift in signal toward the filiform apparatus upon
301 fertilisation as observed for wild-type pollinated ovules. Therefore, under our growth conditions,
302 NTA relocalisation at pollen tube arrival is also affected by a loss of LRE.

303 As reported by Ngo and colleagues (2014), the journey of the pollen tube does not conclude upon
304 contact with the filiform apparatus of the synergid cells [21]. Pollen tubes transiently arrest growth
305 upon contact with the synergid; they then grow rapidly along the receptive synergid and towards
306 the chalazal end, before burst and release of the sperm cells [21]. To observe this process in
307 detail, we used TdTomato-tagged pollen and monitored NTA-GFP localisation at different stages of
308 pollen tube growth within the ovule. The shift in NTA-GFP localisation was noted in ovules in which
309 the pollen tube had grown past the filiform apparatus and ruptured, rather than upon pollen tube
310 arrival at the filiform apparatus (Appendix Figure S6A). Interestingly, in rare cases when pollen
311 tube burst occurred normally in the *herk1 anj* background, the fluorescence shift towards the
312 micropyle had also taken place (Appendix Figure S6A). In both cases, NTA-GFP did not appear to
313 accumulate in the filiform apparatus (Appendix Figure S6B). Our results differ from the
314 interpretation of previous reports that NTA is polarly relocalised from endomembrane
315 compartments to the plasma membrane in the filiform apparatus, instead supporting a more
316 generalised relocalisation within the synergid cytoplasm towards the micropylar end, at least under
317 our growth conditions. We propose that *HERK1*, *ANJ* and *LRE*, similarly to *FER*, act upstream of
318 NTA relocalisation in the signalling pathway.

319 **ROS production is not affected in mature *herk1 anj* ovules**

320 ROS levels in *fer-4* and *lre-5* ovules have been reported to be significantly lower than in wild-type
321 with the implication that, as hydroxyl free radicals can induce pollen tube burst [20], reduced ROS

322 levels could be responsible for pollen tube overgrowth. To assess whether HERK1 and ANJ also
323 act upstream of ROS accumulation in the ovules, we used H₂DCF-DA to measure ROS levels on a
324 categorical scale in *herk1 anj*, *lre-5* and *fer-4* ovules (Appendix Figure S7A,B). To ensure that all
325 ovules were fully developed prior to ROS measurement, we emasculated stage 14 flowers and
326 allowed them to develop for a further 20 hours. At 20 hours after emasculation (HAE), all ovules
327 had reached the mature 7-celled or 4-celled pollen-receptive stages and presented callose
328 accumulation at the filiform apparatus in all backgrounds tested (Figure 4A, S7C, S8; [32,33]).
329 Across three independent experiments, we confirmed that ROS levels are significantly lower in *fer-*
330 *4* ovules compared to wild-type (Figure 4B), indicating that the ROS assay is functional in our
331 hands and able to distinguish changes in ROS levels. However, we found that ROS levels are
332 consistently comparable to wild-type in mature ovules of *herk1 anj* and *lre-5* (Figure 4B). To verify
333 that the fertilisation defect is not rescued in the *herk1 anj* and *lre-5* genotypes at 20 HAE, we
334 confirmed that pollen tube overgrowth still occurs when ovules are fertilised at this stage (Figure
335 4C). Taken together, these results suggest that FER acts upstream of ROS accumulation in ovules
336 prior to pollen tube arrival while, under our experimental conditions, HERK1, ANJ and LRE are not
337 required for this process. As these results conflict with a previous study showing lower ROS levels
338 in *lre-5* ovules [20], this suggests that the function of LRE in ROS production may be
339 environmentally sensitive. Our results do not preclude that pollen tube arrival-induced ROS
340 signalling in the synergid cells is affected in *herk1 anj* and *lre-5*, however differences in transient
341 synergid-specific ROS burst cannot be quantified in our *in vitro* system.

342 **HERK1 and ANJ interact with LRE and FER**

343 LRE and its homolog LORELEI-LIKE GPI-ANCHORED PROTEIN 1 (LLG1) physically interact with
344 RLKs FER, FLAGELLIN SENSING 2 (FLS2) and EF-TU RECEPTOR (EFR) [18,34]. Mutations in
345 these GPI-anchored proteins and their associated RLKs result in similar phenotypes, with LRE and
346 LLG1 regarded as co-receptors and/or stabilisers of RLK function [18,34,35]. HERK1, ANJ and
347 FER are closely related RLKs and, given the similarities in reproduction defects and sub-cellular
348 localisation in synergid cells (Figure 3A), we hypothesised that HERK1 and ANJ may act in

349 complex with LRE and/or FER at the filiform apparatus. To examine this hypothesis, we used yeast
350 two hybrid assays to test for direct interactions between the extracellular juxtamembrane domains
351 of HERK1, ANJ (HERK1exJM, ANJexJM) and LRE, as well as the complete extracellular domains
352 of HERK1, ANJ and FER (HERK1-ECD, ANJ-ECD and FER-ECD). Interactions between
353 HERK1exJM and ANJexJM with LRE were detected, as were interactions of FER-ECD and
354 HERK1-ECD with FER-ECD, HERK1-ECD and ANJ-ECD, and of ANJ-ECD with FER-ECD and
355 HERK1-ECD, indicative of a possible direct interaction between these four proteins (Figure 5A-B).
356 Weaker interactions of HERK1-ECD and FER-ECD with ANJ-ECD, and the lack of interaction of
357 ANJ-ECD with itself could indicate that they do not form complexes *in vivo* or could be the result of
358 a lower expression in yeast of the activation domain (AD) version of ANJ-ECD (ANJ-ECD-AD) in
359 comparison with its HERK1-ECD and FER-ECD counterparts (Figure S9A). Interactions were also
360 tested by yeast two hybrid assays between the kinase domains of HERK1, ANJ and FER (HERK1-
361 KIN, ANJ-KIN and FER-KIN) but interaction between these domains was much weaker (Figure
362 S9B).

363 To corroborate interactions of HERK1, ANJ, FER and LRE *in planta*, co-immunoprecipitation
364 assays were performed. In a heterologous system using *Agrobacterium*-mediated transient
365 expression of *pFER::HERK1-GFP*, *pFER::ANJ-GFP* and *p35S::HA-LRE* in *Nicotiana benthamiana*
366 leaves, HA-LRE co-immunoprecipitated with HERK1-GFP and ANJ-GFP (Figure 5C), confirming
367 that these proteins form complexes *in planta*. Furthermore, *herk1 anj* lines complemented with
368 *pFER::HERK1-GFP* were used to assay the association of HERK1 with endogenous FER using an
369 α -FER antibody [35]. FER co-immunoprecipitated with both HERK1-GFP independent
370 transformants in several independent experiments (Figure 5D), again confirming that these
371 complexes form *in planta*. In an additional genetic approach, we introduced the *lre-5* mutation into
372 the *herk1 anj* background and characterised fertility impairment in triple homozygous *herk1 anj lre-*
373 *5* plants. No additive effect was observed in the seed set defect in *herk1 anj lre-5* plants compared
374 to *herk1 anj* and *lre-5* mutants (Figure EV4A).

375 ROS production in ovules of the triple *herk1 anj lre-5* mutant was measured using H₂DCF-DA at 20
376 HAE. In agreement with the seed set phenotype, ROS levels were unaffected in the triple

377 homozygous line (Figure EV4B). These results reinforce the hypothesis that HERK1, ANJ and LRE
378 act in the same signalling pathway and, given their cellular localisation and our protein-protein
379 interaction results, we propose that HERK1-LRE-FER and ANJ-LRE-FER form part of a receptor
380 complex in the filiform apparatus of synergid cells which mediates pollen tube reception.

381 To test for any additional additive interaction between HERK1, ANJ, FER and LRE at the level of
382 seed set, CRISPR-Cas9 was used with two guide RNAs to generate deletions in *FER* in wild-type,
383 *herk1 anj* and *herk1 anj lre-5* genetic backgrounds. Plants were selected based on the *fer*
384 phenotype. PCR genotyping was used to check each line for deletions, however only two of the
385 eight lines showed smaller PCR bands (Figure EV5A). No PCR products could be amplified for
386 lines 5 or 27 in the *herk1 anj* background, even when primers at least 1.7 kb upstream and 1.1 kb
387 downstream of the two target sites were used (Figure EV5B), which is interpreted as these lines
388 containing larger deletions or inversions than expected. Amplified PCR products were sequenced
389 in the other lines to characterise each of the CRISPR-Cas9 lines, and ranged from single
390 nucleotide insertions which caused a frame shift, to an inversion and deletions (Figure EV5C).
391 Seed set was analysed in T2 plants grown in parallel with wild-type, *herk1 anj*, *lre-5*, *fer-4* and
392 *herk1 anj lre-5* mutants, with further analysis of pollen tube overgrowth in selected lines. No
393 statistically significant difference was found between single, double, triple or quadruple mutants,
394 while all mutants produced significantly fewer seeds and higher levels of pollen tube overgrowth
395 than wild-type (Figure EV5D,E).

396 It has been reported for several mutations causing pollen tube overgrowth, including *lre* and *fer*,
397 that pollen tube overgrowth is occasionally accompanied by polytubey, where more than one
398 pollen tube enters the ovule (Figure EV4C; [16,19]). This is indicative of uninterrupted secretion of
399 attraction signals from the synergid cells, suggesting impaired degeneration of the receptive
400 synergid cell upon pollen tube arrival [36,37]. Polytubey has been reported to occur at a rate of
401 ~10% in the progeny of a heterozygous *fer-1* mutant (Huck Dev 2003). To assess whether
402 polytubey occurs in the *herk1 anj* mutant at a similar rate, polytubey was quantified in *herk1 anj*
403 mutants along with *lre-5* and *fer-4* mutants as controls (Figure EV4D). Under our growth conditions
404 polytubey was more frequent in *fer-4* mutants (38.6% of fertilized ovules) than previously reported
16

405 for *fer-1*. Compared to *fer-4*, *herk1 anj* (24.8% of fertilized ovules) and *lre-5* mutants (27.2% of
406 fertilized ovules) exhibited statistically lower rates of polytubey, whereas *herk1 anj lre-5* mutants
407 presented similar rates to *fer-4* (40.3% of fertilised ovules), indicating that mutations in *HERK1*,
408 *ANJ* and *LRE* may have an additive effect in the attraction of supernumerary pollen tubes.

409

410 **Discussion**

411 Successful reproduction in angiosperms relies on tightly controlled communication between
412 gametophytes through the exchange of chemical and mechanical cues [1]. Here, we describe the
413 role of the RLKs *HERK1* and *ANJ* in early stages of fertilisation in *Arabidopsis*. *HERK1* and *ANJ*
414 are widely expressed in female reproductive tissues including the synergid cells of ovules, where
415 they are polarly localised to the filiform apparatus. *herk1 anj* plants fail to produce seeds from most
416 ovules due to a maternally-derived pollen tube overgrowth defect. As female gametophytes
417 develop normally in *herk1 anj* mutants, pollen tube overgrowth is likely due to impaired signalling.
418 To clarify the position of *HERK1/ANJ* in relation to the previously characterised signalling elements
419 of the pollen tube reception pathway, we have shown that NTA relocalisation after pollen tube
420 reception is impaired in *herk1 anj* as described for *FER*, whereas ROS production at the micropylar
421 entrance of ovules prior to pollen arrival is not affected. Interactions between *HERK1/ANJ*, *FER*
422 and *LRE* lead us to propose receptor complexes containing *HERK1-LRE-FER* and *ANJ-LRE-FER*
423 at the filiform apparatus.

424 Associated with diverse hormonal, developmental and stress responses, *FER* is regarded as a
425 connective hub of cellular responses through its interactions with multiple partners, including small
426 secreted peptides, cell wall components, other RLKs, GPI-anchored proteins and ROPGEFs
427 [18,38-42]. As related members of the *CrRLK1L* family, *HERK1* and *ANJ* have the potential to
428 perform similar roles to *FER*, and as reported here control pollen tube rupture. Interestingly, control
429 of tip growth in pollen tubes depends on two redundant pairs of *CrRLK1L*s: *ANX1* and *ANX2*; and
430 *BUPS1* and *BUPS2* [11-14]. *ANX1/2* and *BUPS1/2* form *ANX-BUPS* heterodimers to control pollen

431 tube growth by sensing autocrine RALF signals [12]. In turn, ovular RALF34 efficiently induces
432 pollen tube rupture at the pollen tip, likely through competition with autocrine RALF4/19 [12].
433 LEUCINE-RICH REPEAT EXTENSINS (LRXs) constitute an additional layer of regulation during
434 pollen tube growth [14]. LRXs interact physically with RALF4/19 and are thought to facilitate RALF
435 sensing during pollen tube growth [14,43,44]. Here we propose that female control of pollen tube
436 reception is executed by an analogous mechanism, where *CrRLK1L* heterocomplexes of FER with
437 either HERK1 or ANJ potentially sense pollen tube-derived cues to trigger the female gametophyte
438 to induce pollen tube rupture. Given the multiple *CrRLK1L*-RALF interactions identified to date
439 [12,14,38,45], pollen tube-derived RALF signals constitute a potential candidate to induce synergid
440 responses to pollen tube perception. RALF4/19 are continuously secreted at the growing tip of the
441 pollen tube and, while their involvement in pollen growth has been thoroughly studied [12,14], their
442 possible dual role as synergid-signalling activators remains unexplored. Disruption of synergid
443 autocrine RALF signalling upon pollen arrival constitutes another possible model, comparable to
444 that hypothesised for RALF34 and RALF4/19 during pollen growth [12]. Additionally, LRXs could
445 facilitate RALF perception at the synergid cell to control pollen tube reception.

446 A second category of putative pollen tube cues involves changes in cell wall properties of the
447 filiform apparatus. As a polarised fast-growing structure, pollen tubes present cell walls that differ
448 from stationary cell types, with particular emphasis on the growing tip where active cell wall
449 remodelling rapidly takes place [46]. When the growing tip reaches the filiform apparatus, it
450 temporarily arrests growth, subsequently growing along the receptive synergid cell prior to rupture
451 [21]. The prolonged direct physical contact between the growing tip and the filiform apparatus likely
452 allows a direct exchange of signals which could result in modification of the filiform apparatus cell
453 wall structure. *CrRLK1L* receptors present an extracellular malectin-like domain [47], a tandem
454 organisation of two malectin domains with structural similarity to the di-glucose binding malectin
455 protein [48]. The malectin di-glucose binding residues are not conserved in the malectin-like
456 domains of ANX1/2 according to structural data [49,50]. However, direct interactions of FER,
457 ANX1/2 and BUPS1/2 malectin-like domains with the pectin building block polygalacturonic acid
458 have been recently reported [39,51]. An extracellular domain anchored to cell wall components

459 and a cytoplasmic kinase domain capable of inducing downstream signalling make FER and the
460 other *CrRLK1L* proteins a putative link between cell wall status and cellular responses [52].
461 Involvement of FER in root mechanosensing provides additional support for this hypothesis [53].
462 Therefore, FER and the related receptors HERK1 and ANJ may be fulfilling a cell wall integrity
463 surveillance function in the filiform apparatus, triggering cellular responses upon changes in the
464 composition or mechanical forces registered at this specialised cell wall structure.

465 Receptor complexes are a common feature in signal transduction in multiple cellular processes
466 [54-56]. Our genetic and biochemical results support possible HERK1-LRE-FER/ANJ-LRE-FER
467 heterocomplexes (Fig. 5 and Fig. 6). LRE and related proteins form complexes with RLKs FER,
468 FLS2 and EFR, making them versatile co-receptors that mediate signal perception in multiple
469 processes [18,34]. LRE functions in the maternal control of fertilisation and early seed
470 development [57,58], whereas its homolog LLG1 is restricted to vegetative growth and plant-
471 pathogen interactions [34]. Uncharacterised LLG2 and LLG3 show pollen-specific expression in
472 microarray data and therefore constitute likely candidates as ANX1/2 and BUPS1/2 receptor
473 complex partners to control pollen tube growth. LRE proteins are thought to stabilise their receptor
474 partners in the plasma membrane and act as direct co-receptors for the extracellular cues sensed
475 by the RLK [18,35]. As we found that FER localisation in the filiform apparatus is unaltered in *lre-5*
476 plants, with HERK1/ANJ localisation also not affected, our results do not support the role
477 previously reported for LRE as a chaperone for FER localisation in synergid cells [18]. A strict
478 requirement for LRE as a FER chaperone in the synergid cells has also been challenged by a
479 previous report evidencing that the fertility defect in *lre* female gametophytes could be partially
480 rescued by pollen-expressed LRE [59]. In the absence of synergid-expressed LRE, the authors
481 speculate that sufficient FER is still localised to the filiform apparatus to interact with LRE on the
482 pollen tube plasma membrane, demonstrating a more minor role for LRE intracellular activity in the
483 synergid cells to correctly localise FER [59]. We hypothesise that LRE could act as co-receptor for
484 FER and HERK1 or ANJ at the filiform apparatus, forming tripartite HERK1-LRE-FER or ANJ-LRE-
485 FER complexes that sense pollen-derived ligands such as RALF peptides or cell wall components,
486 in a mechanism analogous to that described for pollen tube growth through BUPS1/2-ANX1/2-

487 LLG2/3-RALF4/19 signalling. Further verification of the protein-protein interactions described here
488 could be done via Förster Resonance Energy Transfer (FRET) analysis, cryo-electron microscopy
489 [60], or super-resolution microscopy techniques such as Stimulated Emission-Depletion
490 Measurements (STED; [61]).

491 Confirmation of the role of *CrRLK1Ls* and LRE proteins as RALF peptide sensors has been
492 recently obtained through an elegant combination of crystallographic and biochemical techniques
493 [35]. By solving the structure of a FER-LLG1-RALF23 complex, Xiao and colleagues have
494 demonstrated that i) LRE proteins play a central role in the recognition of RALFs; ii) the N-terminal
495 region of a subgroup of RALFs is sufficient to induce the interaction between LRE proteins and
496 FER; iii) while LLG1-3 proteins are capable of binding RALF23, interaction between LRE and
497 RALF23 was not detected; and iv) how specific amino acid differences between LRE and LLG1-3
498 proteins are responsible for such affinity differences [35]. These findings reinforced the hypothesis
499 that signalling specificity can be achieved by the combinatorial action of different *CrRLK1Ls*, LRE
500 proteins, RALFs, and their respective expression patterns and affinities towards each other. Pollen
501 tube reception provides another layer of complexity to this scenario, as two independent cellular
502 systems come into contact, with two putative RALF-sensing complexes (BUPS1/2-ANX1/2-
503 LLG2/3; HERK1/ANJ-FER-LRE) and RALF peptides secreted from both the pollen tube tip and the
504 female gametophyte are brought together. The differences in affinity towards certain RALFs
505 observed between LRE and LLG1-3 allows us to speculate that the pollen derived RALF4/19 may
506 not activate HERK1/ANJ-FER-LRE signalling, and rather this activation may instead depend on
507 maternally-derived RALFs. Detailed dissection of the affinity of LRE towards pollen and ovule-
508 derived RALFs will shed light on how pollen tube reception is mediated. Additionally, while the
509 molecular nature of the tripartite *CrRLK1L*-LRE protein-RALF complex is now well understood,
510 data presented in this report and previous studies point at *CrRLK1L*-to-*CrRLK1L* direct interactions
511 [12], for which structural data remains elusive. It will be necessary to address how these higher
512 order complexes are formed, whether there are tripartite complexes composed by two *CrRLK1Ls*
513 and a single LRE protein, or whether two *CrRLK1L*-LRE protein heterodimers dimerise to form a
514 functional signalling unit.

515 Our results indicate that HERK1, ANJ and LRE are not required to generate the ROS-enriched
516 environment in the micropyle of mature ovules under our experimental conditions, while FER is
517 involved in this process (Fig. 4; [20]). The role of FER in ROS production has also been
518 characterised in root hairs, where FER activates NADPH oxidase activity via ROPGEF and
519 RAC/ROP GTPase signalling, ensuring root hair growth stability [40]. Micropylar ROS
520 accumulation prior to pollen tube arrival depends on NADPH oxidase activity and FER, suggesting
521 a similar pathway to root hairs may take place in synergid cells [20]. This evidence places FER
522 upstream of ROS production, whereas FER, HERK1/ANJ and LRE would function upstream of
523 pollen tube reception. One possible explanation is that FER is a dual regulator in synergid cells,
524 promoting ROS production and regulating pollen tube reception, while HERK1/ANJ and LRE
525 functions are restricted to the latter under our environmental conditions. Kinase-inactive mutants of
526 FER rescue the pollen tube overgrowth defect in *fer* mutants, but cannot restore the sensitivity to
527 exogenous RALF1 in root elongation [62]. These recent findings support multiple signal
528 transduction mechanisms for FER in a context-dependent manner [62]. It would thus be
529 informative to test whether the kinase-inactive version of FER can restore the ovular ROS
530 production defect in *fer* mutants. The use of genetic ROS reporters expressed in synergid cells and
531 pollen tubes in live imaging experiments would allow us to observe specific changes in ROS
532 production at the different stages of pollen tube perception in ovules, as performed with Ca²⁺
533 sensors [21,63,64]. ROS production and Ca²⁺ pump activation in plant cells have been linked
534 during plant-pathogen interactions and are thought to take place during gametophyte
535 communication [65,66]. Thus, given the dynamic changes in Ca²⁺ during the different stages of
536 pollen tube reception in synergids and pollen, it is likely that ROS production variations also take
537 place in parallel. Studying ROS production profiles during pollen perception in the *fer-4*, *herk1 anj*
538 and *lre-5* backgrounds would provide the resolution required to link these receptors to dynamic
539 ROS regulation during pollen reception. Induction of specific Ca²⁺ signatures in the synergids upon
540 pollen tube arrival is dependent on FER, LRE and NTA [21]. Given that NTA relocalisation after
541 pollen reception depends on functional HERK1/ANJ and NTA is involved in modulating Ca²⁺

542 signatures in the synergids, it is possible that HERK1 and ANJ might also be required for Ca²⁺
543 signalling during pollen perception.

544 Downstream signalling after pollen tube reception in the synergid cells likely involves interactions
545 of HERK1, ANJ and FER with cytoplasmic components through their kinase domain. Our results
546 indicate that the kinase activity of HERK1/ANJ is not required for controlling pollen tube rupture
547 (Fig. S4B), as has been reported for FER [29]. The *fer-1* pollen tube overgrowth defect could also
548 be rescued with a chimeric protein comprising the FER extracellular domain and the HERK1
549 kinase domain [29]. This implies that the FER and HERK1/ANJ kinase domains are likely
550 redundant in controlling pollen tube reception and may transduce the signal in a similar manner.
551 Testing whether FER-dependent induction of ROS production in the micropyle is also independent
552 of its kinase activity and whether the HERK1/ANJ kinase domains can also substitute for the FER
553 kinase domain in this process would provide insight into how this signalling network is organised.

554 Our results suggest a model where FER and LRE form functionally redundant complexes with
555 HERK1 and ANJ in the plasma membrane of synergid cells (Figure 6A, B). These complexes could
556 sense maternally- or paternally-derived RALF peptides as has been characterised for analogous
557 protein complexes involved in pollen tube growth. Alternatively, the HERK1/ANJ-FER-LRE
558 complexes may sense changes in cell wall integrity through mechanosensing. As kinase inactive
559 versions of FER can rescue the pollen tube reception phenotype in *fer*, and kinase inactive HERK1
560 or ANJ can likewise complement a *herk1-1 anj-1* mutant, we envisage four possible signalling
561 scenarios (Figure 6C). Firstly, the kinase activity of at least one CrRLK1L receptor may be required
562 for activation of downstream signalling through phosphorylation. Secondly, the kinase activity of
563 none of the CrRLK1L receptors may be required if they act as a scaffold to recruit cytoplasmic
564 kinases. Thirdly, additional receptor kinases (either CrRLK1L or other families) may be present in
565 the complex and be phosphorylated by either FER, or HERK1/ANJ to then activate downstream
566 signalling. And lastly, if we combine scenarios two and three, additional receptor kinases along
567 with the HERK1/ANJ-FER-LRE complex could recruit cytoplasmic kinases to trigger downstream
568 events. Thus a number of scenarios exist for the function of HERK and ANJ in pollen tube
569 reception.

570 This study provides evidence for the involvement of multiple *CrRLK1L* detectors of pollen tube
571 arrival at the female gametophyte, implicating *HERK1* and *ANJ* as co-receptors of *FER*. The action
572 of multiple *CrRLK1L* proteins at the filiform apparatus highlights the relevance of the *CrRLK1L*s in
573 controlling reproduction in flowering plants. Future research in this field will undoubtedly provide
574 new views on how these RLKs integrate pollen-derived cues to ensure tight control of fertilisation.

575

576 **Methods**

577 **Experimental Model and Subject Details**

578 **Plant material.** *Arabidopsis thaliana* T-DNA insertion lines *herk1* (At3g46290; N657488; *herk1-1*;
579 [24]), and *anj* (At5g59700; N654842; *anj-1*) were obtained from the Nottingham Arabidopsis Stock
580 Centre (NASC; [67,68]), along with: *cap1/eru* (At5g61350; N666567), *the1* (At5g54380; N829966),
581 At2g23200 (N685400), *cvy1* (At3g39360;N660329), *herk2* (At1g30570; N663563), *fer* (At3g51550;
582 N655026), *anx1* (At3g04690; N659315) and *anx2* (At5g28680; N656997). T-DNA lines *fer-4*
583 (At3g51550; N69044; [20,38]) and *lre-5* (At4g26466; N66102; [57]) were kindly provided by Prof.
584 Alice Cheung (University of Massachusetts) and Dr. Ravi Palanivelu (University of Arizona),
585 respectively. Accession Col-0 was used as a wild-type control in all experiments. T-DNA lines were
586 confirmed as homozygous for the insertion by genotyping PCRs. The *anj* mutant line was
587 characterised as a knockout of gene expression in this study by RT-qPCR. A full list of plant lines
588 used in this study is given in Appendix Table S1.

589 **Growth conditions.** Seeds were stratified at 4°C for three days. Seeds were sown directly on soil
590 and kept at high humidity for four days until seedlings emerged. The soil mix comprised a 4:1 (v:v)
591 mixture of Levington M3 compost:sand. Plants were grown in walk-in Conviron growth chambers
592 with 22°C continuous temperature, 16 hours per day of ~120 $\mu\text{mol s}^{-1}\text{m}^{-2}$ light and 60% humidity.
593 For selection of transformants, seeds were surface sterilised with chlorine gas, sown onto half-
594 strength Murashige and Skoog medium (MS; [69]), 0.8% (w/v) agar, pH 5.7 (adjusted with KOH),
595 supplemented with the appropriate antibiotic (25 $\mu\text{g/mL}$ of hygromycin B or 50 $\mu\text{g/mL}$ of
23

596 kanamycin). Seeds on plates were stratified for three days at 4°C and then transferred to a growth
597 chamber (Snijders Scientific) at 22°C, 16 hours per day of ~90 $\mu\text{mol}\cdot\text{s}^{-1}\cdot\text{m}^{-2}$ of light. Basta selection
598 was carried out directly on soil soaked in a 1:1000 dilution of Whippet (150 g/L glufosinate
599 ammonium; AgChem Access Ltd).

600 **Method Details**

601 **Phenotyping.** To quantify seed production, fully expanded green siliques were placed on double-
602 sided sticky tape, valves were dissected along the replum with No. 5 forceps, exposing the
603 developing seeds. Dissected siliques were kept in a high humidity chamber until photographed to
604 avoid desiccation. Alternatively, mature siliques were collected prior to dehiscence and cleared in
605 0.4 M NaOH, 1% Triton X-100 for at least two days before imaging with a Microtec dissection
606 microscope. Seeds were counted from the micrographs.

607 Carpels from self-pollinated or hand-pollinated flowers at stage 16 were selected for aniline blue
608 staining of pollen tubes. Carpels were fixed at least overnight in a 3:1 solution of ethanol:acetic
609 acid, then softened overnight in 8 M NaOH, washed four times in water and incubated for three
610 hours in aniline blue staining solution (0.1% (w/v) aniline blue (Fisons Scientific) in 0.1 M K_2PO_4 -
611 KOH buffer, pH 11). Stained carpels were mounted in 50% glycerol, gently squashed onto the
612 microscope slide and then visualised with epifluorescence or confocal microscopy. Aniline blue
613 fluorescence was visualised on a Leica DM6 or Olympus BX51 epifluorescence microscope using
614 a 400 nm LED light source and a filter set with 340-380 nm excitation, emission filter of 425 nm
615 (long pass) and 400 nm dichroic mirror. Confocal images were acquired using a 403.5 nm laser
616 line, 30.7 μm pinhole size and filter set with 405 nm dichroic mirror and 525/50 nm emission filter
617 cube.

618 Quick callose staining was carried out by incubating freshly dissected tissue samples in a 1000x
619 dilution of SR2200 (Renaissance Chemicals Ltd) in half-strength MS, 5% (w/v) sucrose, pH 5.7.
620 Samples were mounted in the staining solution directly and visualised under an epifluorescence
621 microscope with the same settings as used for aniline blue staining. Callose-enriched structures

622 like pollen tubes and the filiform apparatus of ovules display a strong fluorescence within 10
623 minutes of incubation. Only structures directly exposed to the SR2200 solution are stained.

624 To observe the development of the female gametophyte, we used the confocal laser scanning
625 microscopy method as described by Christensen [70]. Ovules were dissected from unpollinated
626 carpels, fixed for 2 hours in a 4% (v/v) solution of glutaraldehyde, 12.5 mM sodium cacodylate
627 buffer pH 6.9, dehydrated in an ethanol series (20%-100%, 20% intervals, 30 minutes each) and
628 cleared in a benzyl benzoate:benzyl alcohol 2:1 mixture for 2 hours prior to visualisation. Samples
629 were mounted in immersion oil, coverslips sealed with clear nail varnish and visualised with an
630 inverted Nikon A1 confocal microscope. Fluorescence was visualised with 35.8 μm pinhole size,
631 642.4 nm laser line and filter set of 640 nm dichroic mirror and 595/50 nm emission filter cube.
632 Multiple z-planes were taken and analysed with ImageJ.

633 Analyses of expression patterns of *HERK1* and *ANJ* used *promoter::reporter* constructs.
634 *promoter::GUS* reporters were analysed by testing β -glucuronidase activity in Col-0 plants from the
635 T1 and T2 generations. Samples were fixed in ice-cold 90% acetone for 20 minutes, then washed
636 for 30 minutes in 50 mM NaPO_4 buffer pH 7.2. Samples were transferred to X-Gluc staining
637 solution (2 mM X-Gluc (Melford Laboratories Ltd), 50 mM NaPO_4 buffer pH 7.2, 2 mM potassium
638 ferrocyanide, 2 mM potassium ferricyanide and 0.2% (v/v) Triton-X), vacuum-infiltrated for 30
639 minutes and incubated at 37°C for several hours or overnight. Samples were cleared in 75%
640 ethanol and visualised under a light microscope or stereomicroscope. For the *promoter::H2B-*
641 *TdTomato* reporters, unpollinated ovules were dissected from the carpels and mounted in half-
642 strength MS, 5% (w/v) sucrose, pH 5.7. RFP signal was detected on a Leica DM6 epifluorescence
643 microscope using a 535 nm LED light source and a filter set with 545/25 nm excitation filter, 605/70
644 nm emission filter and a 565 nm dichroic mirror. DIC images were taken in parallel.

645 $\text{H}_2\text{DCF-DA}$ staining of ROS in ovules was carried out as per [20]. Ovules from unpollinated carpels
646 were dissected and incubated in staining solution (25 μM $\text{H}_2\text{DCF-DA}$ (Thermo Scientific), 50 mM
647 KCl, 10 mM MES buffer pH 6.15) for 15 minutes. Samples were subsequently washed three times
648 in $\text{H}_2\text{DCF-DA}$ -free buffer for 5 minutes, mounted on slides and immediately visualised by

649 epifluorescence microscopy. H₂DCF-DA fluorescence was visualised using a 470 nm LED light
650 source and a filter set with 470/40 nm excitation filter, 460/50 nm emission filter and 495 nm
651 dichroic mirror.

652 All steps were performed at room temperature unless otherwise specified. Ovules were dissected
653 by placing carpels on double-sided sticky tape, separating the ovary walls from the replum with a
654 0.3 mm gauge needle, and by splitting the two halves of the ovary along the septum with No. 5
655 forceps. GFP was visualised by epifluorescence microscopy with the same settings used to
656 visualise H₂DCF-DA fluorescence. TdTomato was visualised as described above.

657 **Cloning and transformation of Arabidopsis.** To study the cellular localisation and to
658 complement the pollen overgrowth defect we generated the constructs *pANJ::ANJ-GFP*,
659 *pHERK1::HERK1*, *pFER::FER-GFP*, *pANJ::ANJ-KD-GFP*, and *pHERK1::HERK1-KD*. Genomic
660 regions of interest (spanning 2 kb upstream of the start codon ATG and the full coding sequence
661 excluding stop codon) were amplified by PCR with Phusion DNA polymerase (NEB).
662 *Promoter::CDS* amplicons were cloned via KpnI/BamHI restriction sites into a pGreen-IIS
663 backbone (Basta resistance; from Detlef Weigel's group, Max Planck Institute for Developmental
664 Biology; [71]), with or without an in-frame C-terminal GFP coding sequence. Kinase-dead versions
665 of *HERK1* and *ANJ* were generated by site-directed mutagenesis of the activation loop residues
666 D606N/K608R of ANJ and D609N/K611R of HERK1 using *pANJ::ANJ-GFP* and *pHERK1::HERK1*
667 constructs as template [72]. To generate the GUS and H2B-TdTomato reporter constructs,
668 *pHERK1* and *pANJ* (from 2 kb upstream of the ATG start codon) were cloned with a pENTR-
669 dTOPO system (Thermo Scientific) and then transferred to the GUS expression cassette in the
670 pGWB433 destination vector or pAH/GW:H2B-TdTomato via LR recombination (LR clonase II;
671 Thermo Scientific; [73]). ASE *Agrobacterium tumefaciens* strain was used with pGreen vectors;
672 GV3101pMP90 strain was used otherwise. Arabidopsis stable transformants were generated
673 through the floral dip method. Primers used for cloning are listed in Appendix Table S2 and all
674 plasmids used in this study are listed in Appendix Table S3.

675 To test interaction *in vivo* in co-immunoprecipitation assays, we generated *pFER::ANJ-GFP* via
676 three-way ligation cloning of KpnI-*pFER*-NotI and NotI-*ANJ*-BamHI fragments into a pGreen-IIS
677 backbone (Basta resistance; from Detlef Weigel's group, Max Planck Institute for Developmental
678 Biology; [71]). To test direct interaction between HERK1exJM, ANJexJM and LRE in yeast, we
679 cloned the extracellular juxtamembrane sequence corresponding to the 81 amino acids N-terminal
680 of the predicted transmembrane domain of HERK1 and ANJ, as well as the sequence
681 corresponding to the amino acids 23-138 of LRE [as per [18]]. Interaction between HERK1, ANJ
682 and FER was also assayed by Y2H and the extracellular domains excluding the signal peptide
683 (HERK1-ECD, amino acids 24-405; ANJ-ECD, amino acids 25-405; FER-ECD, amino acids 28-
684 446) as well as the cytosolic kinase domains (HERK1-KIN, amino acids 429-830; ANJ-KIN, amino
685 acids 429-830; FER-KIN, amino acids 470-895). Amplicons of exJM and KIN domains were cloned
686 into yeast two hybrid vectors pGADT7 and pGBKT7 via SmaI restriction digests, in frame with the
687 activation or DNA binding domains (AD or BD, respectively). Amplicons of ECD domains were
688 cloned into PCR8 entry vectors and subsequently recombined into pGADT7-GW and pGBKT7-GW
689 via LR recombination. Col-0 genomic DNA was used as the template for all cloning events unless
690 otherwise specified.

691 To mutate *FER* in the Col-0, *herk1 anj* and *herk1 anj lre* genotypes, CRISPR-Cas9 with two guide
692 RNAs was used to generate large deletions. The guide RNAs were designed with
693 <https://crispr.dbcls.jp> to target two regions of the *FER* gene 1.7 to 2.2 kb apart and were cloned
694 into pBEE401E. T1 transformants were selected with BASTA and based on a *fer-4*-like phenotype.
695 Seed set was assessed in the T2 generation and the lines genotyped at *FER* to verify either a
696 large deletion in the gene or no amplification due to loss of the primer binding sites. Primers used
697 for cloning are listed in Appendix Table S2.

698 For the kinase assays, the cytosolic domains (CDs) of WT or kinase-dead (KD) variants of HERK1
699 (amino acids 429-830) or ANJ (amino acids 429-829) were cloned into the pOPINM expression
700 vector in frame with an N-terminal 6xHis-maltose binding protein (-MBP) tag using InFusion
701 clonase (Takara) using the pOM primers listed in Appendix Table S2.

702 **Genotyping PCRs and RT-qPCRs.** Genomic DNA was extracted from leaves of 2-week old
703 seedlings by grinding fresh tissue in DNA extraction buffer (200 mM Tris-HCl pH 7.5, 250 mM
704 NaCl, 25 mM EDTA and 0.5% SDS), precipitating DNA with isopropanol, washing pellets with 75%
705 EtOH and resuspending DNA in water. Genotyping PCRs were performed with Taq polymerase
706 and 35 cycles with 60°C annealing temperature and one minute extension time. RNA was
707 extracted a Spectrum Plant Total RNA extraction kit (Sigma) for qPCR, from 100 mg of floral tissue
708 from three plants per line. RNA concentrations were normalised, an aliquot was DNaseI-treated
709 and subsequently transcribed into first strand cDNA with the RevertAid cDNA synthesis kit
710 (Thermo Scientific) using random hexamers. qPCRS were performed on a Qiagen Rotor-Gene Q
711 machine (40 cycles of 95°C for 10 seconds to denature and 60°C for 40 seconds to anneal and
712 extend) using a Rotor-Gene SYBR Green PCR kit (Qiagen). Expression was standardised to actin.
713 Primers for genotyping and qPCR are listed in the Appendix Table S2.

714 **Yeast two-hybrid assays.** Direct interaction assays in yeast were carried out following the
715 Clontech small-scale LiAc yeast transformation procedure. Yeast strain Y187 was transformed with
716 pGADT7 constructs and yeast strain Y2HGold with pGBKT7 constructs (including empty vectors
717 as controls). Yeast diploids cells carrying both plasmids were obtained by mating and interaction
718 tests were surveyed on selective media lacking leucine, tryptophan and histidine.

719 FER-, HERK1- and ANJ-ECD protein fusions to the Gal4-BD and Gal4-AD were detected by
720 Western blots with antibodies anti-Myc (1:1000 dilution, clone 9E10; Roche) and anti-HA (clone
721 3F10; Roche), respectively. For yeast protein extraction, cultures (OD600 0.7) were centrifuged
722 and the pellets resuspended in sterile water. 0.2 M NaOH was used immediately to lyse the cells
723 for 5 min at room temperature. After centrifugation, pellets were resuspended in Laemmli 1X buffer
724 (0.034 M Tris-HCl pH 6.8, 1% SDS, 12.5% glycerol, 0.0075% bromophenol blue, 1 M 1,4-
725 dithiothreitol (DTT)) and heat to 95°C for 3 minutes. Extracts were centrifuged and the
726 supernatants collected and stored at -80°C. 5 µg total protein of each sample was loaded on the
727 gel.

728 **Co-immunoprecipitation and western blots.** For assays using transient expression, leaves of
729 4.5-week-old *N. benthamiana* were infiltrated with *A. tumefaciens* strain GV3101 carrying
730 constructs indicated in figure captions. In all cases, leaves were co-infiltrated with *A. tumefaciens*
731 carrying a P19 silencing suppressor. Leaves were harvested 2 days post-infiltration and frozen in
732 liquid nitrogen before extraction in buffer (20 mM MES pH 6.3, 100 mM NaCl, 10% glycerol, 2 mM
733 EDTA, 5 mM DTT, supplemented with 1% IGEPAL and protease inhibitors). Immunoprecipitations
734 were performed in the same buffer with 0.5% IGEPAL for 3-4 hours at 4°C with GFP-trap resin
735 (Chromotek). Beads were washed 3 times with the same buffer and bound proteins were eluted by
736 addition of SDS loading dye and heating to 90°C for 10 min. Proteins were separated by SDS-
737 PAGE and detected via Western blot following blocking (in TBS 0.1% Tween-20 with 5% non-fat
738 milk powder) with the following antibody dilutions in the same blocking solution: α-GFP-HRP (B-2,
739 sc-9996, Santa Cruz), 1:5000; α-HA-HRP (3F10, Roche), 1:3000.

740 To test whether HERK1 associates with FER *in planta*, T2 generation *herk1 anj* lines expressing
741 *pFER::HERK1-GFP* were germinated on selection for 5 days. Homozygous *p35S::Lti6b-GFP* (Col-
742 0 background) was used as a control membrane-localized GFP-tagged protein [74]. 5-day-old
743 seedlings were transferred to liquid MS culture and grown in 6-well plates for an additional 7 days.
744 Seedlings were harvested and ground in liquid nitrogen and total protein was extracted in IP buffer
745 (50 mM Tris-Cl pH 7.5, 150 mM NaCl, 2 mM EDTA, 10% glycerol, supplemented with 5 mM DTT,
746 0.5 mM PMSF, Sigma protease inhibitor cocktail P9599, and Sigma phosphatase inhibitor cocktails
747 2 and 3) + 1% IGEPAL. Extracts were clarified by centrifugation at 10,000g, filtered through
748 Miracloth (Millipore), and diluted with detergent-free IP buffer to 0.5% IGEPAL (final concentration).
749 Immunoprecipitations were performed with GFP-trap resin (Chromotek) for 4 hours at 4°C with
750 mixing. Beads were collected by centrifugation at 500g and washed three times with IP buffer +
751 0.5% IGEPAL. Bound proteins were eluted by heating to 80°C in 2x SDS-loading dye. FER was
752 detected using anti-FER (rabbit polyclonal, 1:1000;[35]) and anti-Rabbit IgG (whole molecule)-
753 HRP (Sigma A0545, 1:5000).

754 **Recombinant protein expression, purification, and kinase assays.** 6xHis-MBP-CD fusion
755 proteins were expressed in BL21 Rosetta pLysS cells and purified via Ni²⁺-affinity chromatography
29

756 using Ni Sepharose High Performance resin (GE Healthcare). After purification, the proteins were
757 concentrated into buffer (25 mM Tris-Cl pH 7.5, 100 mM NaCl, 2 mM DTT, 10% glycerol) using
758 Amicon centrifugal concentrators (MWCO 10,000. Millipore) and stored at -80°C until use. For
759 kinase assays, 1 µg of 6xHis-MBP-CD was mixed with 1 µg myelin basic protein (MyBP) in a 30 µl
760 reaction in kinase buffer (25 mM Tris-Cl pH 7.5, 3 mM MgCl₂, 3 mM MnCl₂, 1 mM DTT). Reactions
761 were initiated with the addition of 10 µM ATP with 1 µCi ³²P-γ-ATP and were carried out for 30 min
762 at 25°C. Proteins were separated by SDS-PAGE, transferred to PVDF membrane, stained with
763 Coomassie brilliant blue G-250, and imaged using a Typhoon phosphorimager (GE Healthcare).

764 **Microscopy and image building.** Epifluorescence images were obtained with Leica DM6 or
765 Olympus BX51 widefield microscopes equipped with HC PL Fluotar objectives or UPlanFI 4x,10x
766 and 20x objectives, respectively. A Nikon A1 inverted confocal laser scanning microscope fitted
767 with Plan Fluor 40x oil and Plan Apo VC 60x oil objectives was used to obtain confocal
768 micrographs. A Leica M165 FC stereomicroscope was used to visualise floral tissues from GUS
769 stained samples. Leica LASX, NIS Elements Viewer and ImageJ software were used to analyse
770 microscopy images. Inkscape was used to build all figures in this article.

771 **Quantification and Statistical Analysis**

772 Leica LASX software was used to obtain relative fluorescence intensity profiles from synergid cells
773 by defining linear regions of interest across the synergid cytoplasm in a micropylar to chalazal
774 orientation. Synergid cytoplasm area was defined between the filiform apparatus and the synergid-
775 egg cell chalazal limit using the corresponding DIC images.

776 Statistical significance in seed set averages and relative fluorescence averages (at equivalent
777 distances from the filiform apparatus) were assessed with Student's *t*-tests. χ -square tests were
778 used to compare distributions obtained in pollen tube overgrowth assays and ROS measurements
779 in ovules, using the distribution obtained in wild-type plants as the expected distribution. In all
780 tests, **p*<0.05, ***p*<0.01, and ****p*<0.001. When more than 5 comparisons were required, one-way
781 ANOVA was performed using Origin Pro 2017 and 2018b, followed by Tukey's or Bonferroni's
782 tests if differences were detected. Sample size *n* is indicated in the graphs or in figure legends.

783

784 **Acknowledgements**

785 We thank: Andrew Fleming and his group at the University of Sheffield for early feedback and
786 guidance on experiments; Alice Cheung and Qiaohong Duan from the University of Massachusetts
787 for advice on the ROS assays and for sharing *fer-4* seeds with us; Chao Li from East China
788 Normal University for the *p35S::HA-LRE* construct; Ravi Palanivelu from the University of Arizona
789 for *Ire-5* seeds; Martin Bayer from the Max Planck Institute for Developmental Biology for the
790 *pLAT52::TdTomato* line; Ueli Grossniklaus from the University of Zurich for the *pFER::HERK1-*
791 *GFP* and *pLRE::LRE-Citrine* constructs; Sharon Kessler from Purdue University for sharing the
792 *pMYB98::NTA-GFP* construct; Daphne Goring from the University of Toronto for the pBEE401E
793 CRISPR/Cas-9 construct and Melinka Butenko at the University of Oslo for the pAH21\GW vector
794 used to make *promoter::H2B-TdTomato* reporters. S.G-T. was supported by a Department of
795 Animal and Plant Sciences postgraduate teaching fellowship. Research in J.E.G.'s lab is supported
796 by RCUK grant BB/N004167/1. T.A.D. was supported by post-doctoral fellowships from the
797 European Molecular Biology Organisation (LTF 100-2017) and the Natural Sciences and
798 Engineering Research Council of Canada (PDF-532561-19). N.B-T. was supported by a MINECO
799 FPI Fellowship (BES-2014-068868) and we acknowledge David Alabadi for his supervision of N.B-
800 T. The Zipfel laboratory was supported by the Gatsby Charitable Foundation and European
801 Research Council (PEPTALK). Confocal imaging work was performed at the Wolfson Light
802 Microscope Facility using the Nikon A1 confocal microscope.

803

804 **Author contributions:**

805 Conceptualization, S.G-T. and L.M.S.; Methodology, S.G-T. and L.M.S.; Investigation, S.G-T., N.B-
806 T., T.A.D., L.M.S. and E.S.W.; Writing – Original Draft, S.G-T. and L.M.S.; Writing – Review &
807 Editing, all authors; Supervision, C.Z., J.E.G and L.M.S.

808

809 **Declaration of interests**

810 The authors declare that they have no conflict of interest.

811 **Data availability**

812 The protein interactions from this publication have been submitted to the IMEx
813 (<http://www.imexconsortium.org>) consortium through the IntAct Molecular Interaction Database
814 [75], and assigned the identifier IM-27345
815 (<https://www.ebi.ac.uk/intact/search/do/search?searchString=pubid:unassigned2053>).

816 .

817

818 **References**

- 819 1. Dresselhaus T, Sprunck S, Wessel GM (2016) Fertilization Mechanisms in Flowering Plants.
820 *Current Biology* **26**: R125-R139
- 821 2. Johnson MA, Harper JF, Palanivelu R (2019) A Fruitful Journey: Pollen Tube Navigation from
822 Germination to Fertilization. *Annu Rev Plant Biol* **70**: 809-837
- 823 3. Higashiyama T (2002) The synergid cell: attractor and acceptor of the pollen tube for double
824 fertilization. *Journal of Plant Research* **115**: 149-160
- 825 4. Huang B-Q, Russell SD (1992) Female Germ Unit: Organization, Isolation, and Function. *Journal*
826 *140*: 233-293
- 827 5. Okuda S, Tsutsui H, Shiina K, Sprunck S, Takeuchi H, Yui R, Kasahara RD, Hamamura Y, Mizukami
828 A, Susaki D, *et al.* (2009) Defensin-like polypeptide LUREs are pollen tube attractants secreted
829 from synergid cells. *Nature* **458**: 357-361
- 830 6. Zhong S, Liu M, Wang Z, Huang Q, Hou S, Xu YC, Ge Z, Song Z, Huang J, Qiu X, *et al.* (2019)
831 Cysteine-rich peptides promote interspecific genetic isolation in Arabidopsis. *Science* **364**:
- 832 7. Wang T, Liang L, Xue Y, Jia PF, Chen W, Zhang MX, Wang YC, Li HJ, Yang WC (2016) A receptor
833 heteromer mediates the male perception of female attractants in plants. *Nature* **531**: 241-+
- 834 8. Takeuchi H, Higashiyama T (2016) Tip-localized receptors control pollen tube growth and LURE
835 sensing in Arabidopsis. *Nature* **531**: 245-+
- 836 9. Zhang XX, Liu WJ, Nagae TT, Takeuchi H, Zhang HQ, Han ZF, Higashiyama T, Chai JJ (2017)
837 Structural basis for receptor recognition of pollen tube attraction peptides. *Nature*
838 *Communications* **8**: 1331
- 839 10. Franck CM, Westermann J, Boisson-Dernier A (2018) Plant Malectin-Like Receptor Kinases:
840 From Cell Wall Integrity to Immunity and Beyond. *Annu Rev Plant Biol* **69**: 301-328

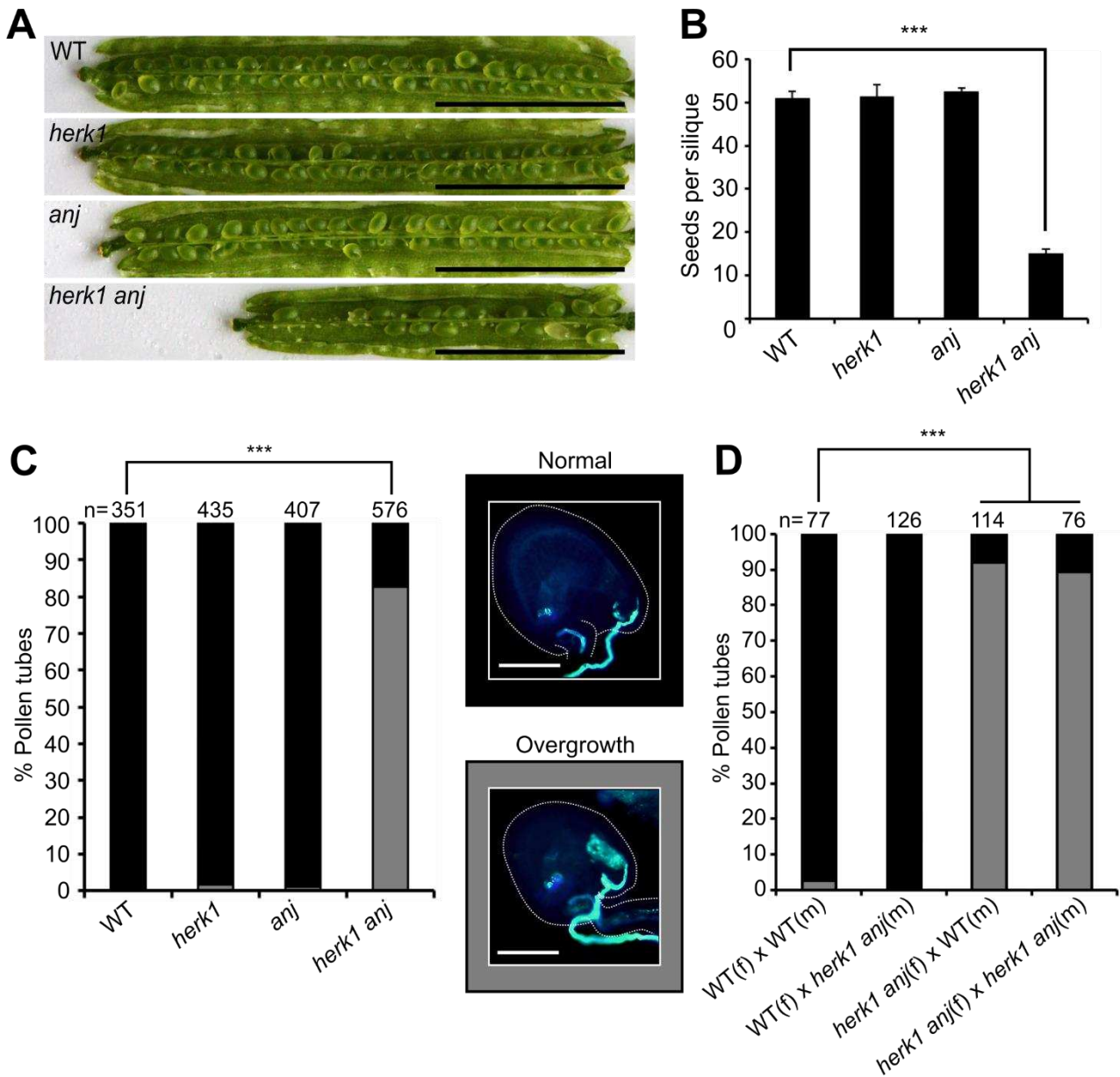
- 841 11. Boisson-Dernier A, Roy S, Kritsas K, Grobei MA, Jaciubek M, Schroeder JI, Grossniklaus U (2009)
842 Disruption of the pollen-expressed FERONIA homologs ANXUR1 and ANXUR2 triggers pollen tube
843 discharge. *Development* **136**: 3279-3288
- 844 12. Ge ZX, Bergonci T, Zhao YL, Zou YJ, Du S, Liu MC, Luo XJ, Ruan H, Garcia-Valencia LE, Zhong S, *et*
845 *al.* (2017) Arabidopsis pollen tube integrity and sperm release are regulated by RALF-mediated
846 signaling. *Science* **358**: 1596-1599
- 847 13. Miyazaki S, Murata T, Sakurai-Ozato N, Kubo M, Demura T, Fukuda H, Hasebe M (2009)
848 ANXUR1 and 2, sister genes to FERONIA/SIRENE, are male factors for coordinated fertilization.
849 *Curr Biol* **19**: 1327-1331
- 850 14. Mecchia MA, Santos-Fernandez G, Duss NN, Somoza SC, Boisson-Dernier A, Gagliardini V,
851 Martinez-Bernardini A, Fabrice TN, Ringli C, Muschietti JP, *et al.* (2017) RALF4/19 peptides interact
852 with LRX proteins to control pollen tube growth in Arabidopsis. *Science* **358**: 1600-1603
- 853 15. Schoenaers S, Balcerowicz D, Costa A, Vissenberg K (2017) The Kinase ERULUS Controls Pollen
854 Tube Targeting and Growth in Arabidopsis thaliana. *Frontiers in Plant Science* **8**: 1942
- 855 16. Huck N, Moore JM, Federer M, Grossniklaus U (2003) The Arabidopsis mutant feronia disrupts
856 the female gametophytic control of pollen tube reception. *Development* **130**: 2149-2159
- 857 17. Escobar-Restrepo JM, Huck N, Kessler S, Gagliardini V, Gheyselinck J, Yang WC, Grossniklaus U
858 (2007) The FERONIA receptor-like kinase mediates male-female interactions during pollen tube
859 reception. *Science* **317**: 656-660
- 860 18. Li C, Yeh FL, Cheung AY, Duan Q, Kita D, Liu MC, Maman J, Luu EJ, Wu BW, Gates L, *et al.* (2015)
861 Glycosylphosphatidylinositol-anchored proteins as chaperones and co-receptors for FERONIA
862 receptor kinase signaling in Arabidopsis. *Elife* **4**: e06587
- 863 19. Capron A, Gourgues M, Neiva LS, Faure J-E, Berger F, Pagnussat G, Krishnan A, Alvarez-Mejia C,
864 Vielle-Calzada J-P, Lee Y-R, *et al.* (2008) Maternal Control of Male-Gamete Delivery in Arabidopsis
865 Involves a Putative GPI-Anchored Protein Encoded by the LORELEI Gene. *The Plant Cell* **20**: 3038-
866 3049
- 867 20. Duan Q, Kita D, Johnson EA, Aggarwal M, Gates L, Wu HM, Cheung AY (2014) Reactive oxygen
868 species mediate pollen tube rupture to release sperm for fertilization in Arabidopsis. *Nat Commun*
869 **5**: 3129
- 870 21. Ngo QA, Vogler H, Lituiev DS, Nestorova A, Grossniklaus U (2014) A Calcium Dialog Mediated
871 by the FERONIA Signal Transduction Pathway Controls Plant Sperm Delivery. *Developmental Cell*
872 **29**: 491-500
- 873 22. Kessler SA, Shimosato-Asano H, Keinath NF, Wuest SE, Ingram G, Panstruga R, Grossniklaus U
874 (2010) Conserved molecular components for pollen tube reception and fungal invasion. *Science*
875 **330**: 968-971
- 876 23. Jones DS, Kessler SA (2017) Cell type-dependent localization of MLO proteins. *Plant Signaling*
877 *& Behavior* **12**: e1393135
- 878 24. Guo H, Li L, Ye H, Yu X, Algreen A, Yin Y (2009) Three related receptor-like kinases are required
879 for optimal cell elongation in Arabidopsis thaliana. *Proc Natl Acad Sci U S A* **106**: 7648-7653
- 880 25. Guo H, Ye H, Li L, Yin Y (2009) A family of receptor-like kinases are regulated by BES1 and
881 involved in plant growth in Arabidopsis thaliana. *Plant Signal Behav* **4**: 784-786
- 882 26. Keinath NF, Kierszniowska S, Lorek J, Bourdais G, Kessler SA, Shimosato-Asano H, Grossniklaus
883 U, Schulze WX, Robatzek S, Panstruga R (2010) PAMP (pathogen-associated molecular pattern)-
884 induced changes in plasma membrane compartmentalization reveal novel components of plant
885 immunity. *J Biol Chem* **285**: 39140-39149
- 886 27. Hematy K, Sado PE, Van Tuinen A, Rochange S, Desnos T, Balzergue S, Pelletier S, Renou JP,
887 Hofte H (2007) A receptor-like kinase mediates the response of Arabidopsis cells to the inhibition
888 of cellulose synthesis. *Curr Biol* **17**: 922-931

- 889 28. Galindo-Trigo S, Gray JE, Smith LM (2016) Conserved Roles of CrRLK1L Receptor-Like Kinases in
890 Cell Expansion and Reproduction from Algae to Angiosperms. *Front Plant Sci* **7**: 1269
- 891 29. Kessler SA, Lindner H, Jones DS, Grossniklaus U (2015) Functional analysis of related CrRLK1L
892 receptor-like kinases in pollen tube reception. *EMBO Rep* **16**: 107-115
- 893 30. Knighton DR, Zheng JH, Teneyck LF, Ashford VA, Xuong NH, Taylor SS, Sowadski JM (1991)
894 Crystal-Structure of the Catalytic Subunit of Cyclic Adenosine-Monophosphate Dependent Protein-
895 Kinase. *Science* **253**: 407-414
- 896 31. Tsukamoto T, Qin Y, Huang YD, Dunatunga D, Palanivelu R (2010) A role for LORELEI, a putative
897 glycosylphosphatidylinositol-anchored protein, in Arabidopsis thaliana double fertilization and
898 early seed development. *Plant Journal* **62**: 571-588
- 899 32. Yadegari R, Drews GN (2004) Female gametophyte development. *Plant Cell* **16**: S133-S141
- 900 33. Christensen CA, Subramanian S, Drews GN (1998) Identification of gametophytic mutations
901 affecting female gametophyte development in Arabidopsis. *Developmental Biology* **202**: 136-151
- 902 34. Shen QJ, Bourdais G, Pan HR, Robotzek S, Tang DZ (2017) Arabidopsis
903 glycosylphosphatidylinositol-anchored protein LLG1 associates with and modulates FLS2 to
904 regulate innate immunity. *P Natl Acad Sci USA* **114**: 5749-5754
- 905 35. Xiao Y, Stegmann M, Han Z, DeFalco TA, Parys K, Xu L, Belkhadir Y, Zipfel C, Chai J (2019)
906 Mechanisms of RALF peptide perception by a heterotypic receptor complex. *Nature* **572**: 270-274
- 907 36. Beale KM, Leydon AR, Johnson MA (2012) Gamete Fusion Is Required to Block Multiple Pollen
908 Tubes from Entering an Arabidopsis Ovule. *Current Biology* **22**: 1090-1094
- 909 37. Maruyama D, Volz R, Takeuchi H, Mori T, Igawa T, Kurihara D, Kawashima T, Ueda M, Ito M,
910 Umeda M, *et al.* (2015) Rapid Elimination of the Persistent Synergid through a Cell Fusion
911 Mechanism. *Cell* **161**: 907-918
- 912 38. Haruta M, Sabat G, Stecker K, Minkoff BB, Sussman MR (2014) A peptide hormone and its
913 receptor protein kinase regulate plant cell expansion. *Science* **343**: 408-411
- 914 39. Feng W, Kita D, Peaucelle A, Cartwright HN, Doan V, Duan QH, Liu MC, Maman J, Steinhorst L,
915 Schmitz-Thom I, *et al.* (2018) The FERONIA Receptor Kinase Maintains Cell-Wall Integrity during
916 Salt Stress through Ca²⁺ Signaling. *Current Biology* **28**: 666-+
- 917 40. Duan Q, Kita D, Li C, Cheung AY, Wu HM (2010) FERONIA receptor-like kinase regulates RHO
918 GTPase signaling of root hair development. *Proc Natl Acad Sci U S A* **107**: 17821-17826
- 919 41. Stegmann M, Monaghan J, Smakowska-Luzan E, Rovenich H, Lehner A, Holton N, Belkhadir Y,
920 Zipfel C (2017) The receptor kinase FER is a RALF-regulated scaffold controlling plant immune
921 signaling. *Science* **355**: 287-289
- 922 42. Hou YN, Guo XY, Cyprys P, Zhang Y, Bleckmann A, Cai L, Huang QP, Luo Y, Gu HY, Dresselhaus T,
923 *et al.* (2016) Maternal ENODLs Are Required for Pollen Tube Reception in Arabidopsis. *Current*
924 *Biology* **26**: 2343-2350
- 925 43. Stegmann M, Zipfel C (2017) Complex regulation of plant sex by peptides. *Science* **358**: 1544-
926 1545
- 927 44. Moussu S, Broyart C, Santos-Fernandez G, Augustin S, Wehrle S, Grossniklaus U, Santiago J
928 (2019) Structural basis for recognition of RALF peptides by LRX proteins during pollen tube growth.
929 *bioRxiv* 695874
- 930 45. Gonneau M, Desprez T, Martin M, Doblaz VG, Bacete L, Miart F, Sormani R, Hématy K, Renou J,
931 Landrein B, *et al.* (2018) Receptor Kinase THESEUS1 Is a Rapid Alkalinization Factor 34 Receptor in
932 Arabidopsis. *Current Biology* **28**: 2452-2458
- 933 46. Chebli Y, Kaneda M, Zerzour R, Geitmann A (2012) The Cell Wall of the Arabidopsis Pollen
934 Tube-Spatial Distribution, Recycling, and Network Formation of Polysaccharides. *Plant Physiology*
935 **160**: 1940-1955
- 936 47. Boisson-Dernier A, Kessler SA, Grossniklaus U (2011) The walls have ears: the role of plant
937 CrRLK1Ls in sensing and transducing extracellular signals. *J Exp Bot* **62**: 1581-1591

- 938 48. Schallus T, Jaeckh C, Feher K, Palma AS, Liu Y, Simpson JC, Mackeen M, Stier G, Gibson TJ, Feizi
939 T, *et al.* (2008) Malectin: a novel carbohydrate-binding protein of the endoplasmic reticulum and a
940 candidate player in the early steps of protein N-glycosylation. *Mol Biol Cell* **19**: 3404-3414
- 941 49. Du S, Qu LJ, Xiao J (2018) Crystal structures of the extracellular domains of the CrRLK1L
942 receptor-like kinases ANXUR1 and ANXUR2. *Protein Sci* **27**: 886-892
- 943 50. Moussu S, Augustin S, Roman AO, Broyart C, Santiago J (2018) Crystal structures of two
944 tandem malectin-like receptor kinases involved in plant reproduction. *Acta Crystallogr D Struct*
945 *Biol* **74**: 671-680
- 946 51. Lin W, Tang W, Anderson C, Yang Z (2018) FERONIA's sensing of cell wall pectin activates ROP
947 GTPase signaling in Arabidopsis. *bioRxiv*
- 948 52. Verger S, Hamant O (2018) Plant Physiology: FERONIA Defends the Cell Walls against
949 Corrosion. *Curr Biol* **28**: R215-R217
- 950 53. Shih HW, Miller ND, Dai C, Spalding EP, Monshausen GB (2014) The Receptor-like Kinase
951 FERONIA Is Required for Mechanical Signal Transduction in Arabidopsis Seedlings. *Current Biology*
952 **24**: 1887-1892
- 953 54. Greeff C, Roux M, Mundy J, Petersen M (2012) Receptor-like kinase complexes in plant innate
954 immunity. *Frontiers in Plant Science* **3**: 209
- 955 55. Burkart RC, Stahl Y (2017) Dynamic complexity: plant receptor complexes at the plasma
956 membrane. *Current Opinion in Plant Biology* **40**: 15-21
- 957 56. Couto D, Zipfel C (2016) Regulation of pattern recognition receptor signalling in plants. *Nature*
958 *Reviews Immunology* **16**: 537
- 959 57. Tsukamoto T, Qin Y, Huang Y, Dunatunga D, Palanivelu R (2010) A role for LORELEI, a putative
960 glycosylphosphatidylinositol-anchored protein, in Arabidopsis thaliana double fertilization and
961 early seed development. *The Plant Journal* **62**: 571-588
- 962 58. Wang YB, Tsukamoto T, Noble JA, Liu XL, Mosher RA, Palanivelu R (2017) Arabidopsis LORELEI,
963 a Maternally Expressed Imprinted Gene, Promotes Early Seed Development. *Plant Physiology* **175**:
964 758-773
- 965 59. Liu X, Castro C, Wang Y, Noble J, Ponvert N, Bundy M, Hoel C, Shpak E, Palanivelu R (2016) The
966 Role of LORELEI in Pollen Tube Reception at the Interface of the Synergid Cell and Pollen Tube
967 Requires the Modified Eight-Cysteine Motif and the Receptor-Like Kinase FERONIA. *Plant Cell* **28**:
968 1035-1052
- 969 60. Miura K (2018) An Overview of Current Methods to Confirm Protein-Protein Interactions.
970 *Protein and peptide letters* **25**: 728-733
- 971 61. Demir F, Horntrich C, Blachutzik JO, Scherzer S, Reinders Y, Kierszniowska S, Schulze WX,
972 Harms GS, Hedrich R, Geiger D, *et al.* (2013) Arabidopsis nanodomain-delimited ABA signaling
973 pathway regulates the anion channel SLAH3. *Proceedings of the National Academy of Sciences*
974 **110**: 8296
- 975 62. Haruta M, Gaddameedi V, Burch H, Fernandez D, Sussman MR (2018) Comparison of the
976 effects of a kinase-dead mutation of FERONIA on ovule fertilization and root growth of
977 Arabidopsis. *FEBS Lett*
- 978 63. Hamamura Y, Nishimaki M, Takeuchi H, Geitmann A, Kurihara D, Higashiyama T (2014) Live
979 imaging of calcium spikes during double fertilization in Arabidopsis. *Nature Communications* **5**:
980 4722
- 981 64. Denninger P, Bleckmann A, Lausser A, Vogler F, Ott T, Ehrhardt DW, Frommer WB, Sprunck S,
982 Dresselhaus T, Grossmann G (2014) Male-female communication triggers calcium signatures
983 during fertilization in Arabidopsis. *Nature Communications* **5**: 4645
- 984 65. Bleckmann A, Alter S, Dresselhaus T (2014) The beginning of a seed: regulatory mechanisms of
985 double fertilization. *Frontiers in Plant Science* **5**: 452

986 66. Ma W, Berkowitz GA (2007) The grateful dead: calcium and cell death in plant innate
987 immunity. *Cell Microbiol* **9**: 2571-2585
988 67. Alonso JM, Stepanova AN, Leisse TJ, Kim CJ, Chen HM, Shinn P, Stevenson DK, Zimmerman J,
989 Barajas P, Cheuk R, *et al.* (2003) Genome-wide Insertional mutagenesis of *Arabidopsis thaliana*.
990 *Science* **301**: 653-657
991 68. Kleinboelting N, Huep G, Kloetgen A, Viehoveer P, Weisshaar B (2012) GABI-Kat SimpleSearch:
992 new features of the *Arabidopsis thaliana* T-DNA mutant database. *Nucleic Acids Research* **40**:
993 D1211-D1215
994 69. Murashige T, Skoog F (1962) A Revised Medium for Rapid Growth and Bio Assays with Tobacco
995 Tissue Cultures. *Physiologia Plantarum* **15**: 473-497
996 70. Christensen CA, King EJ, Jordan JR, Drews GN (1997) Megagametogenesis in *Arabidopsis* wild
997 type and the Gf mutant. *Sex Plant Reprod* **10**: 49-64
998 71. Mathieu J, Warthmann N, Kuttner F, Schmid M (2007) Export of FT protein from phloem
999 companion cells is sufficient for floral induction in *Arabidopsis*. *Current Biology* **17**: 1055-1060
1000 72. Ho SN, Hunt HD, Horton RM, Pullen JK, Pease LR (1989) Site-Directed Mutagenesis by Overlap
1001 Extension Using the Polymerase Chain-Reaction. *Gene* **77**: 51-59
1002 73. Nakagawa T, Suzuki T, Murata S, Nakamura S, Hino T, Maeo K, Tabata R, Kawai T, Tanaka K,
1003 Niwa Y, *et al.* (2007) Improved Gateway Binary Vectors: High-Performance Vectors for Creation of
1004 Fusion Constructs in Transgenic Analysis of Plants. *Bioscience, Biotechnology, and Biochemistry* **71**:
1005 2095-2100
1006 74. Kadota Y, Sklenar J, Derbyshire P, Stransfeld L, Asai S, Ntoukakis V, Jones JD, Shirasu K, Menke
1007 F, Jones A, *et al.* (2014) Direct regulation of the NADPH oxidase RBOHD by the PRR-associated
1008 kinase BIK1 during plant immunity. *Mol Cell* **54**: 43-55
1009 75. Orchard S, Ammari M, Aranda B, Breuza L, Briganti L, Broackes-Carter F, Campbell NH, Chavali
1010 G, Chen C, del-Toro N, *et al.* (2014) The MIntAct project--IntAct as a common curation platform for
1011 11 molecular interaction databases. *Nucleic Acids Res* **42**: D358-363
1012 76. Li C, Yeh FL, Cheung AY, Duan Q, Kita D, Liu MC, Maman J, Luu EJ, Wu BW, Gates L, *et al.* (2015)
1013 Glycosylphosphatidylinositol-anchored proteins as chaperones and co-receptors for FERONIA
1014 receptor kinase signaling in *Arabidopsis*. *Elife* **4**:
1015
1016

1017



1019

1020

1021 **Figure 1. The *herk1 anj* fertility defect is caused by maternally-mediated pollen tube**
 1022 **overgrowth.**

1023 A Representative siliques from wild-type (WT; Col-0), *herk1*, *anj* and *herk1 anj* plants prior to
 1024 dehiscence. Siliques were placed on double-sided sticky tape and carpel walls separated from the
 1025 replum to expose the developing seeds. Scale bar = 5 mm.

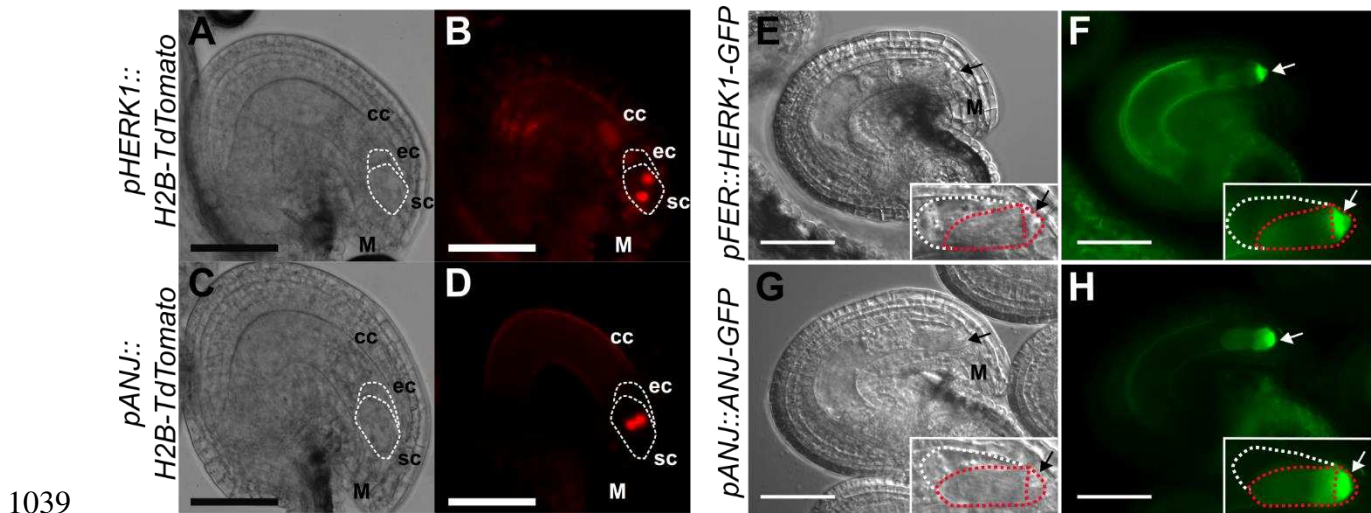
1026 B Developing seeds per silique in wild-type, *herk1*, *anj* and *herk1 anj* plants. Fully expanded
1027 siliques were dissected and photographed under a stereomicroscope. $n = 15$ (four independent
1028 experiments with at least three plants per line and five siliques per plant). Data presented are
1029 means \pm SEM. *** $p < 0.001$ (Student's *t*-test).

1030 C Percentage of pollen tubes with normal reception at the female gametophyte (black bars;
1031 representative image middle centre of figure) and with overgrowth (grey bars; representative image
1032 lower centre) as assessed by aniline blue staining. 15 self-pollinated stage 16 flowers from wild-
1033 type, *herk1*, *anj* and *herk1 anj* were analysed. Legend scale bars = 50 μm . *** $p < 0.001$ (χ -square
1034 tests).

1035 D Aniline blue staining of pollen tube reception in reciprocal crosses between wild-type and *herk1*
1036 *anj* plants with at least two siliques per cross. Legend as per (C). *** $p < 0.001$ (χ -square tests).

1037

1038



1040 **Figure 2. HERK1 and ANJ are expressed in the female gametophyte and localise to the**
 1041 **filiform apparatus of the synergid cells.**

1042 A,B Expression of *pHERK1::H2B-TdTomato* in mature ovules. White dotted lines delineate the egg
 1043 cell and synergid cells.

1044 C,D Expression of *pANJ::H2B-TdTomato* in mature ovules. White dotted lines delineate the egg
 1045 cell and synergid cells.

1046 E,F Localisation of HERK1-GFP in the synergid cell from the *pFER::HERK1-GFP* construct in (F)
 1047 and corresponding differential interference contrast (DIC) image in (E). White and red dotted lines
 1048 delineate the egg cell and synergid cells, respectively.

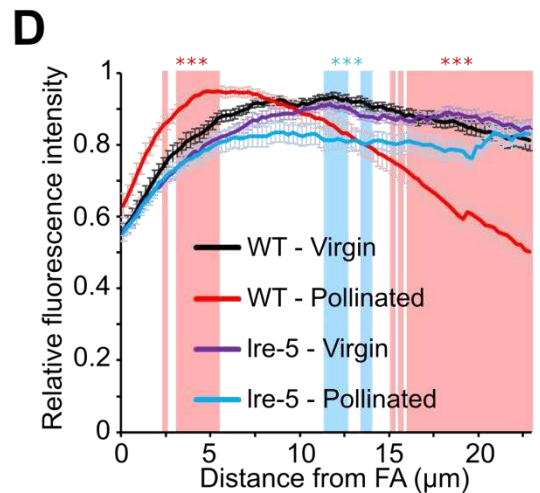
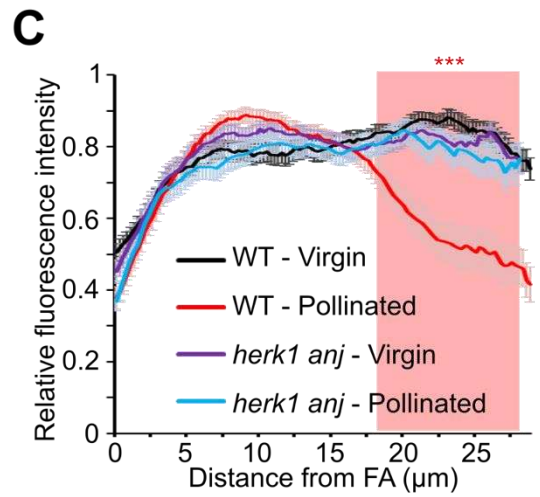
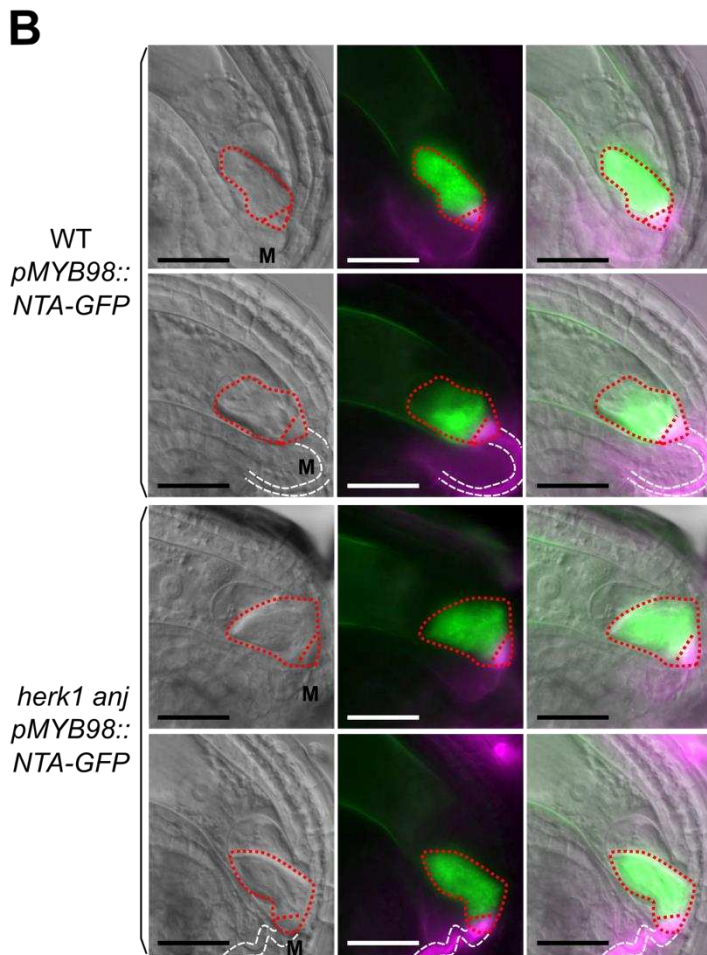
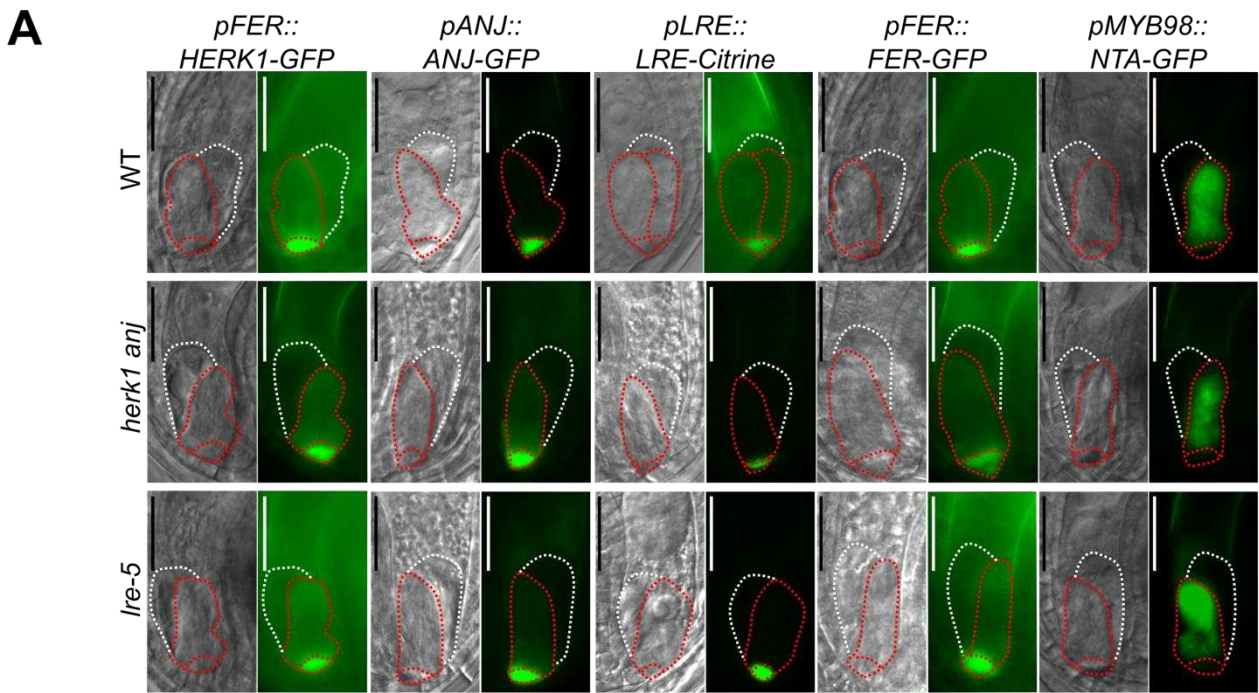
1049 G,H Localisation of ANJ-GFP in the synergid cell from the *pANJ::ANJ-GFP* construct in (H) and
 1050 corresponding DIC image in (G). White and red dotted lines delineate the egg cell and synergid
 1051 cells, respectively.

1052 Scale bars = 50 μ m. M, micropyle. Arrows, filiform apparatus.

1053

1054

1055



1056

1057 **Figure 3. Normal synergid localisation of HERK1, ANJ, LRE, FER and NTA pre-fertilisation**
 1058 **and impaired localisation of NTA after pollen tube reception in *herk1 anj* and *Ire-5*.**

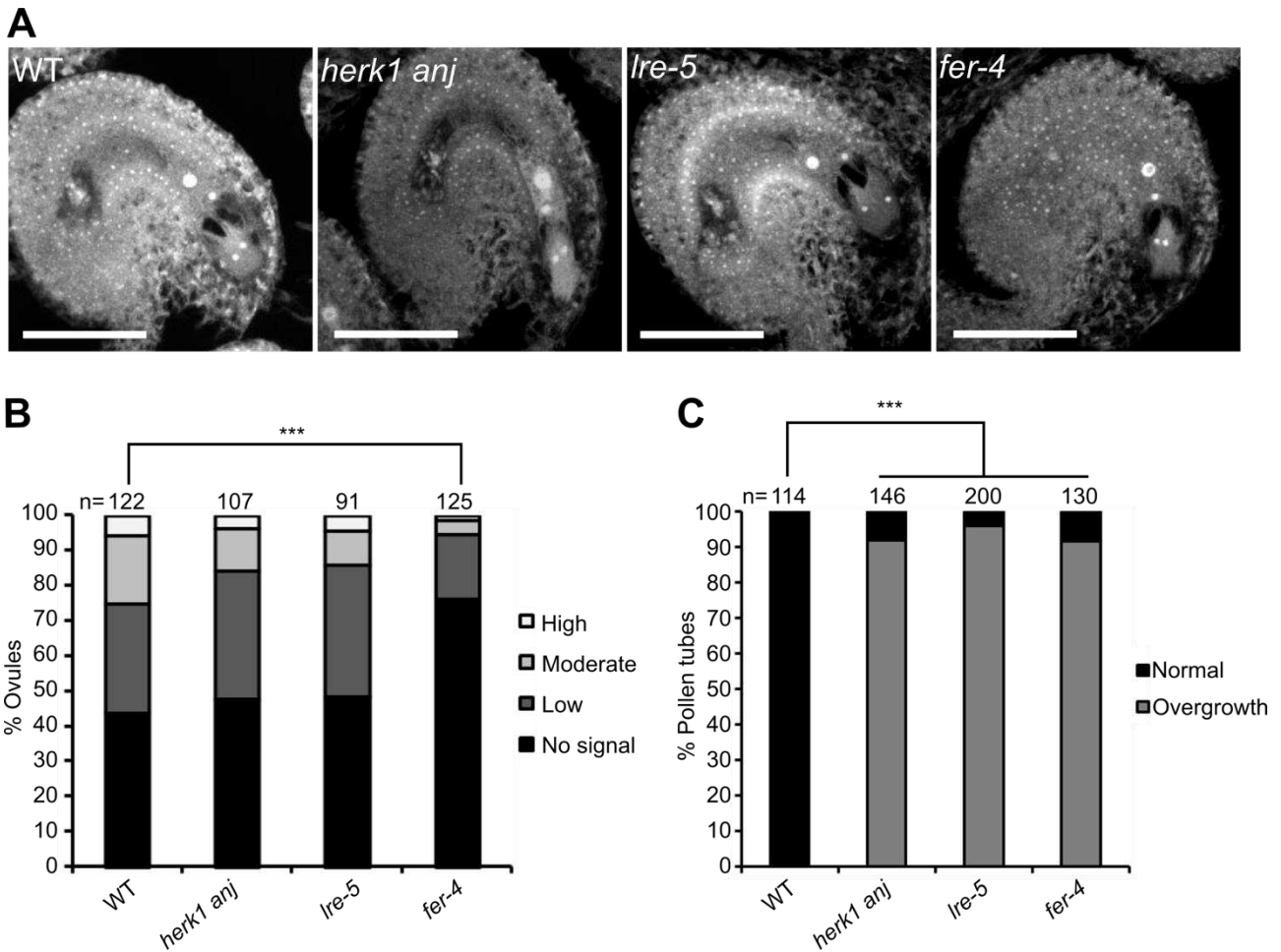
1059 A Localisation of HERK1, ANJ, LRE, FER and NTA in the synergid cell of wild-type (Col-0; WT),
1060 *herk1 anj* and *lre-5* in unfertilised ovules, as shown by *pFER::HERK1-GFP*, *pANJ::ANJ-GFP*,
1061 *pLRE::LRE-Citrine*, *pFER::FER-GFP* and *pMYB98::NTA-GFP*. DIC and fluorescence images are
1062 shown, left to right, respectively. White and red dotted lines delineate the egg cell and synergid
1063 cells, respectively. Scale bars = 25 μ m.

1064 B Localisation of NTA in the synergid cell of wild-type and *herk1 anj* plants before (upper panels)
1065 and after (lower panels) pollen tube arrival. In green, NTA localisation as shown by *pMYB98::NTA-*
1066 *GFP* fluorescence. In magenta, callose of the filiform apparatus and pollen tube stained with
1067 SR2200. From left to right, images shown are DIC, merged fluorescence images, and merged
1068 images of DIC and fluorescence. White and red dotted lines delineate the pollen tube and synergid
1069 cells, respectively. Scale bars = 25 μ m. M, micropyle.

1070 C,D Profile of relative fluorescence intensity of NTA-GFP along the synergid cells of wild-type and
1071 *herk1 anj* ovules (C); and wild-type and *lre-5* ovules (D) before (virgin) and after (pollinated) pollen
1072 arrival. Data shown are means \pm SEM, n = 25. *** $p < 0.001$ (Student's *t*-test). FA, filiform
1073 apparatus.

1074

1075



1076

1077 **Figure 4. *herk1 anj* mature female gametophytes are morphologically normal and**
 1078 **unaffected in ROS production at the micropyle.**

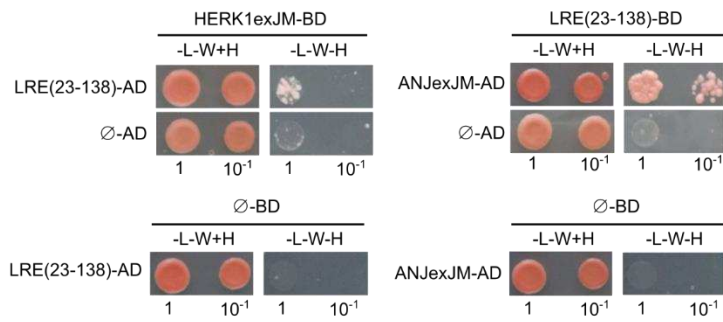
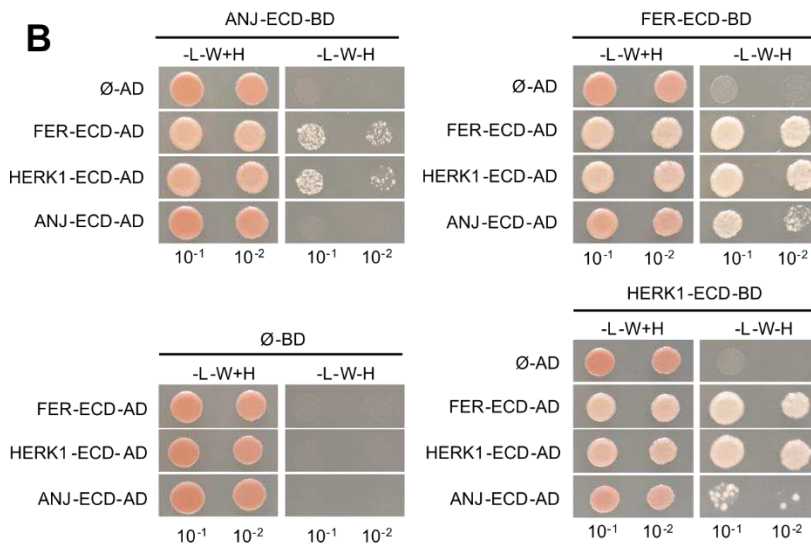
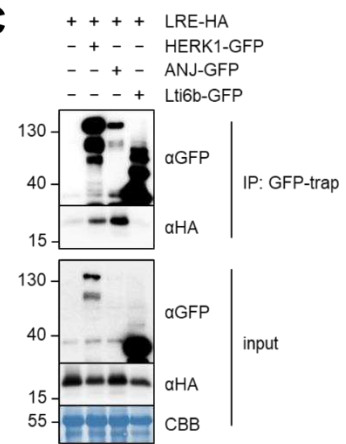
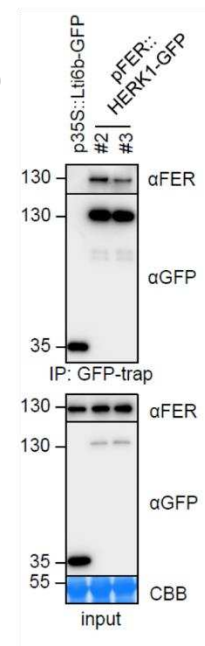
1079 A Representative images of ovules from wild-type (Col-0), *herk1 anj*, *Ire-5* and *fer-4* 20 hours after
 1080 emasculatation (HAE) displaying the mature female gametophyte structure. Images presented here
 1081 are maximum intensity projections from confocal microscopy images across several z-planes of
 1082 ovules stained as per [70]. Scale bars = 50 μ m.

1083 B Quantification of H₂DCF-DA staining of ROS in ovules from wild-type, *herk1 anj*, *Ire-5* and *fer-4*
 1084 plants at 20 HAE. Categories are listed in the legend (see also Appendix Figure S7A). Ovules
 1085 dissected from at least five siliques per line. *** p<0.001 (χ -square tests).

1086 C Percentage of pollen tubes with normal reception at the female gametophyte (black bars) and
 1087 displaying overgrowth (grey bars) in wild-type, *herk1 anj*, *Ire-5* and *fer-4* plants, manually selfed at
 1088 20 HAE. Fertilisation events counted from at least three siliques per line. *** p<0.001 (Student's *t*-
 42

1089 test).

1090

A**B****C****D**

1091

1092 **Figure 5. HERK1 and ANJ interact with LRE and FER.**

1093 A Yeast two hybrid (Y2H) assays of the extracellular juxtamembrane domains of HERK1 and ANJ
 1094 (HERK1exJM and ANJexJM, respectively) with LRE (residues 23-138; signal peptide and C-
 1095 terminal domains excluded).

1096

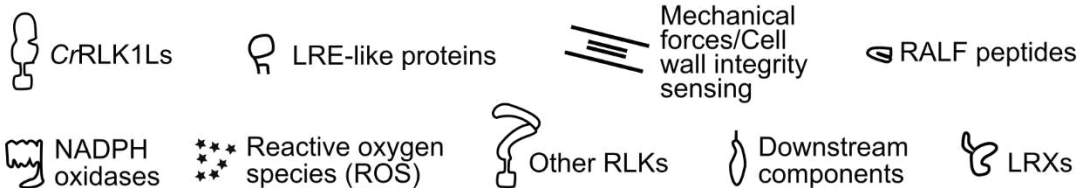
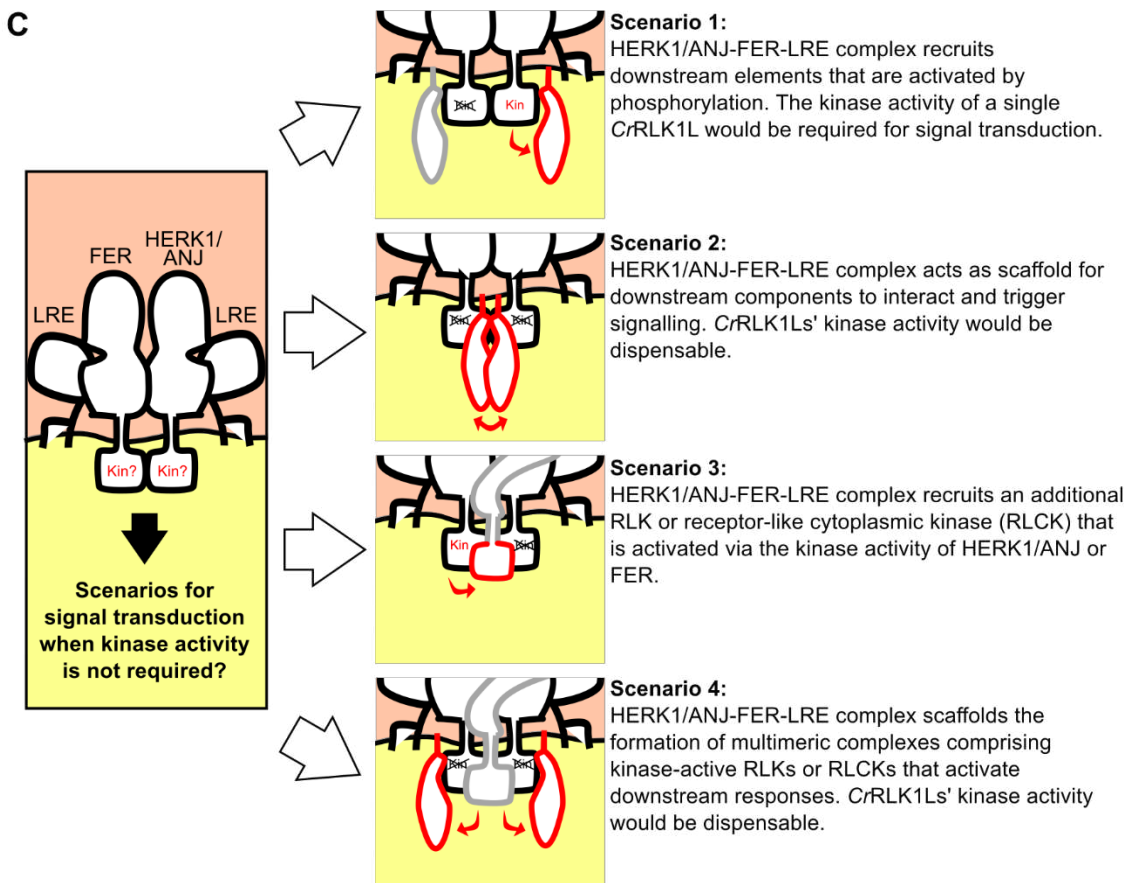
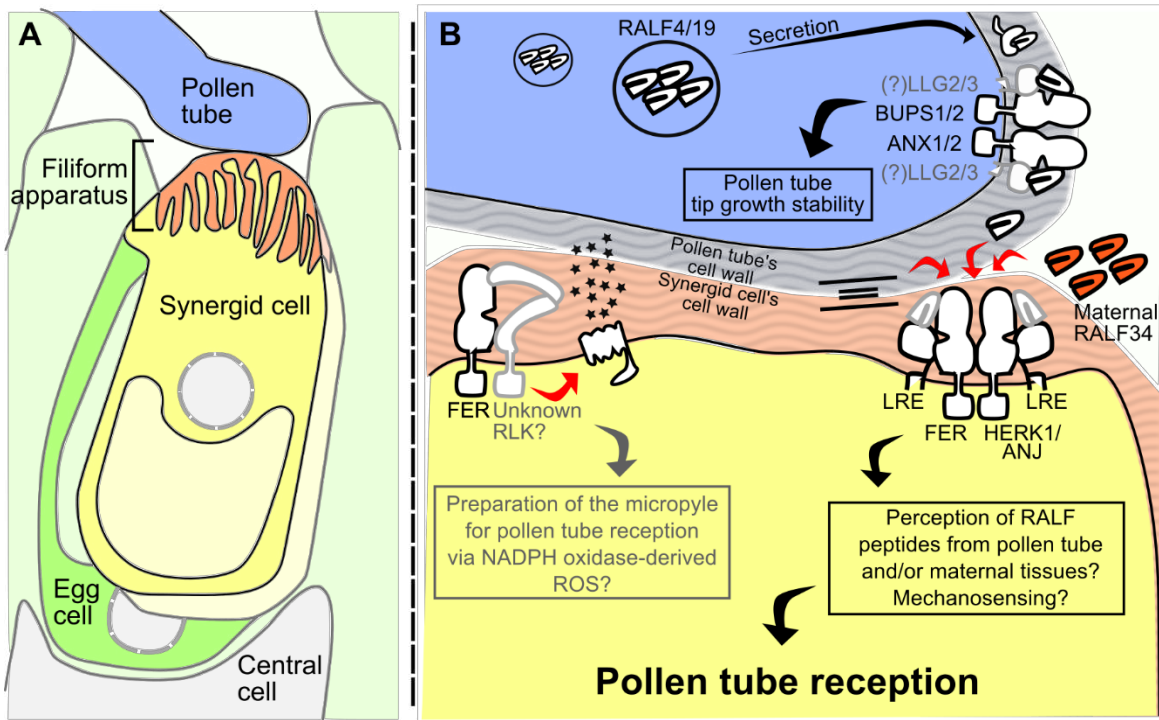
1097 B Y2H assays with the extracellular domains of HERK1, ANJ and FER (HERK1-ECD, ANJ-ECD
 1098 and FER-ECD, respectively). \emptyset represents negative controls where no sequence was cloned into
 1099 the activating domain (AD) or DNA-binding domain (BD) constructs. -L-W-H, growth medium
 1100 depleted of leucine (-L), tryptophan (-W) and histidine (-H).

1101

1102 C Co-immunoprecipitation of HA-LRE with HERK1-GFP or ANJ-GFP following 2 days of transient
1103 expression in *N. benthamiana* leaves.

1104

1105 D Co-immunoprecipitation of FER with HERK1-GFP in Arabidopsis seedlings expressing
1106 *pFER::HERK1-GFP*. Numbers indicate molecular weight marker sizes in kDa. Assays were
1107 performed twice with similar results. CBB refers to Coomassie Brilliant Blue staining of total
1108 proteins.



1110 **Figure 6: Model of HERK1/ANJ involvement in pollen tube reception.**

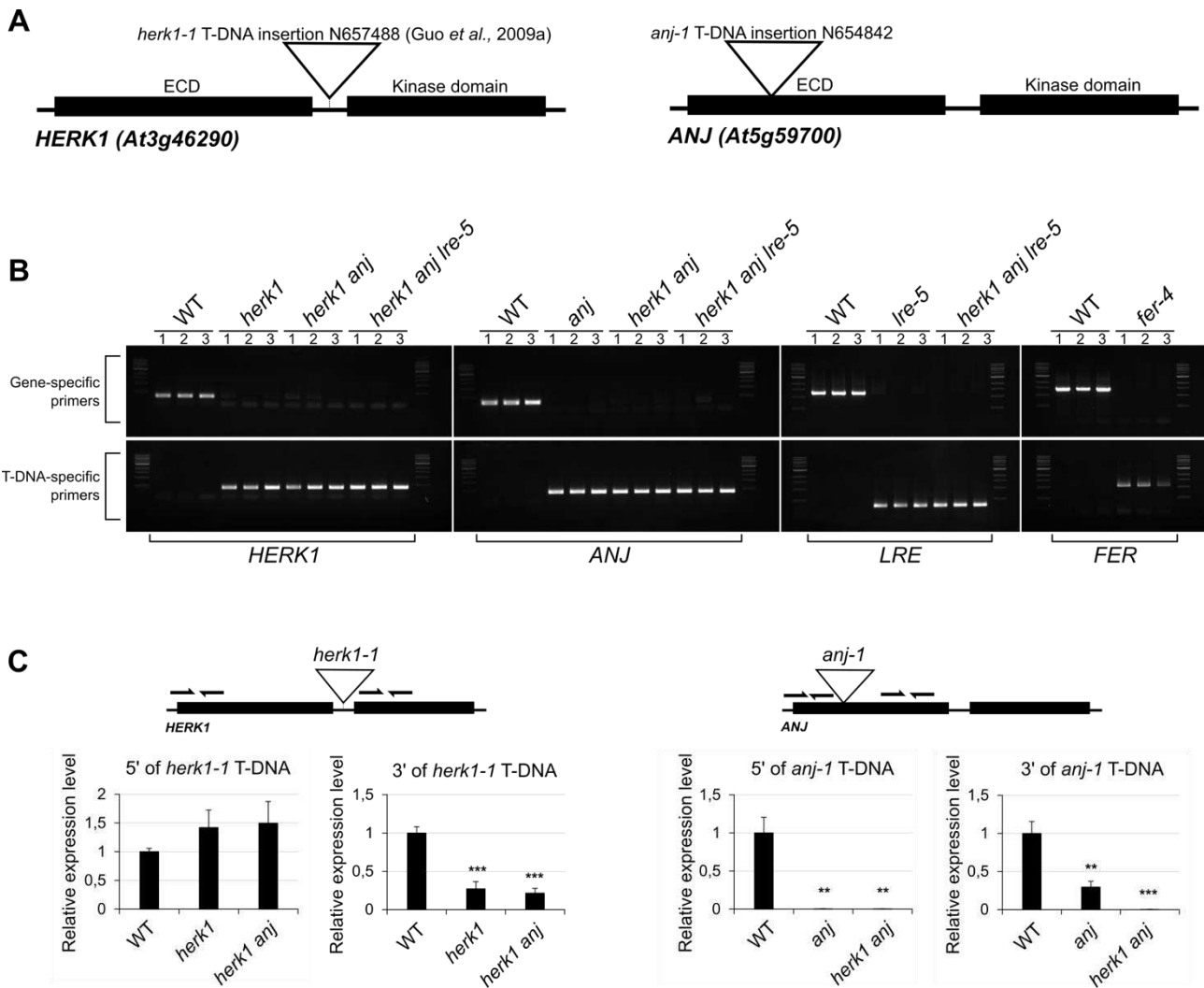
1111 A Overview of the contact point between the male and female gametophytes at pollen tube
1112 reception.

1113 B Proposed mechanism(s) of pollen tube reception at a molecular level where HERK1 and ANJ
1114 form alternative co-receptors with FER and LRE. Unknown components or interactions are shown
1115 in grey. Maternally- or paternally-derived RALFs could act as ligands for the HERK1-LRE-
1116 FER/ANJ-LRE-FER heterocomplexes.

1117 C Four possible scenarios where kinase activity of HERK1/ANJ are not required for signal
1118 transduction during pollen tube reception. Red components indicate proteins active in signal
1119 transduction while black proteins act as scaffolds for complex assembly. Each scenario is
1120 discussed in more detail in the discussion section.

1121

1122 **Expanded view figure legends**



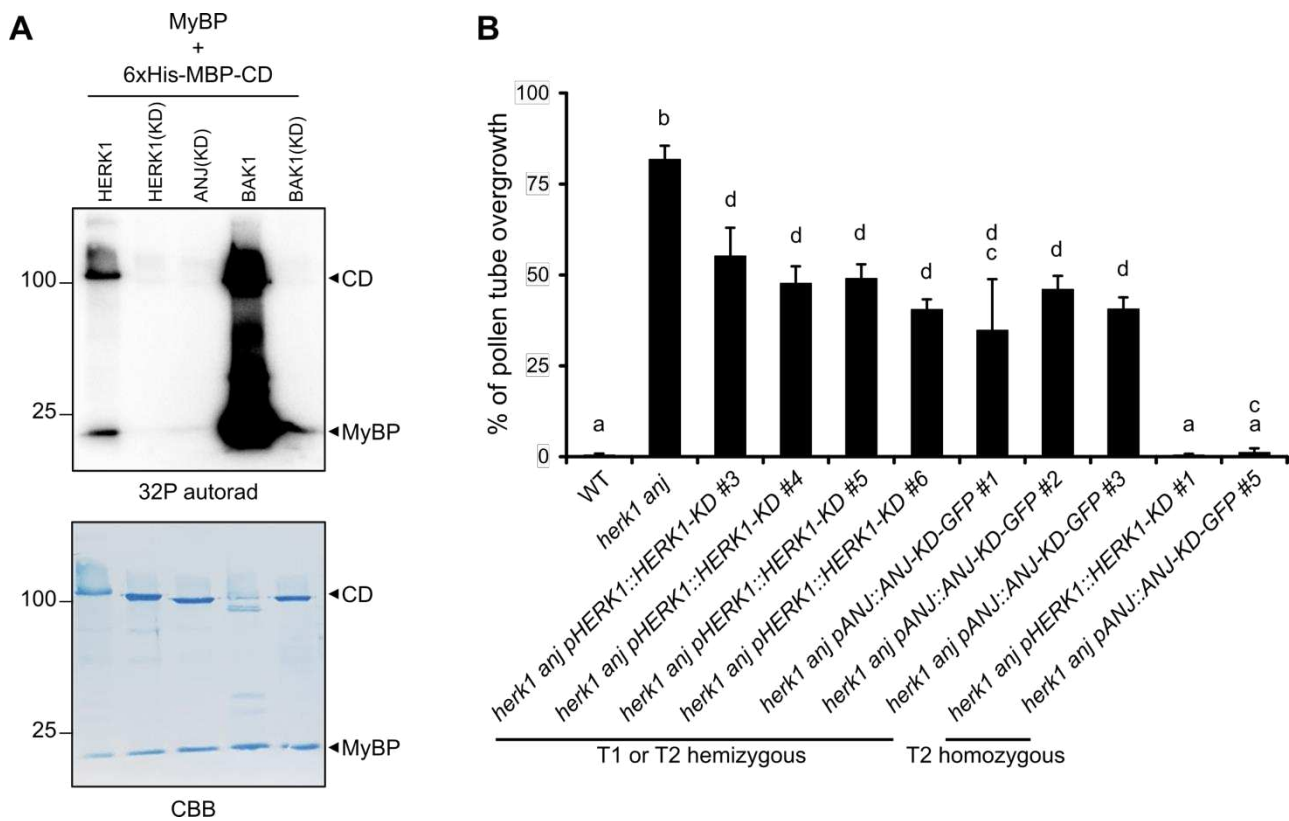
1123

1124 **Figure EV1. Confirmation of *ANJEA* gene expression knock out and genotyping of T-DNA**
 1125 **lines used in this study.**

1126 A Domain organisation of *HERK1* and *ANJEA* and T-DNA insertion sites in the lines used in this
 1127 study, *herk1-1* and *anj-1*.

1128 B Genotyping PCRs to verify homozygosity in the lines used in this study. DNA from three
 1129 independent seedlings per line was analysed.

1130 C RT-qPCR analysis of *HERK1* gene expression in wild-type, *herk1* and *herk1 anj* plants, and *ANJ*
 1131 gene expression in wild-type, *anj* and *herk1 anj* plants. RNA was extracted from multiple
 1132 inflorescences from three plants per line.



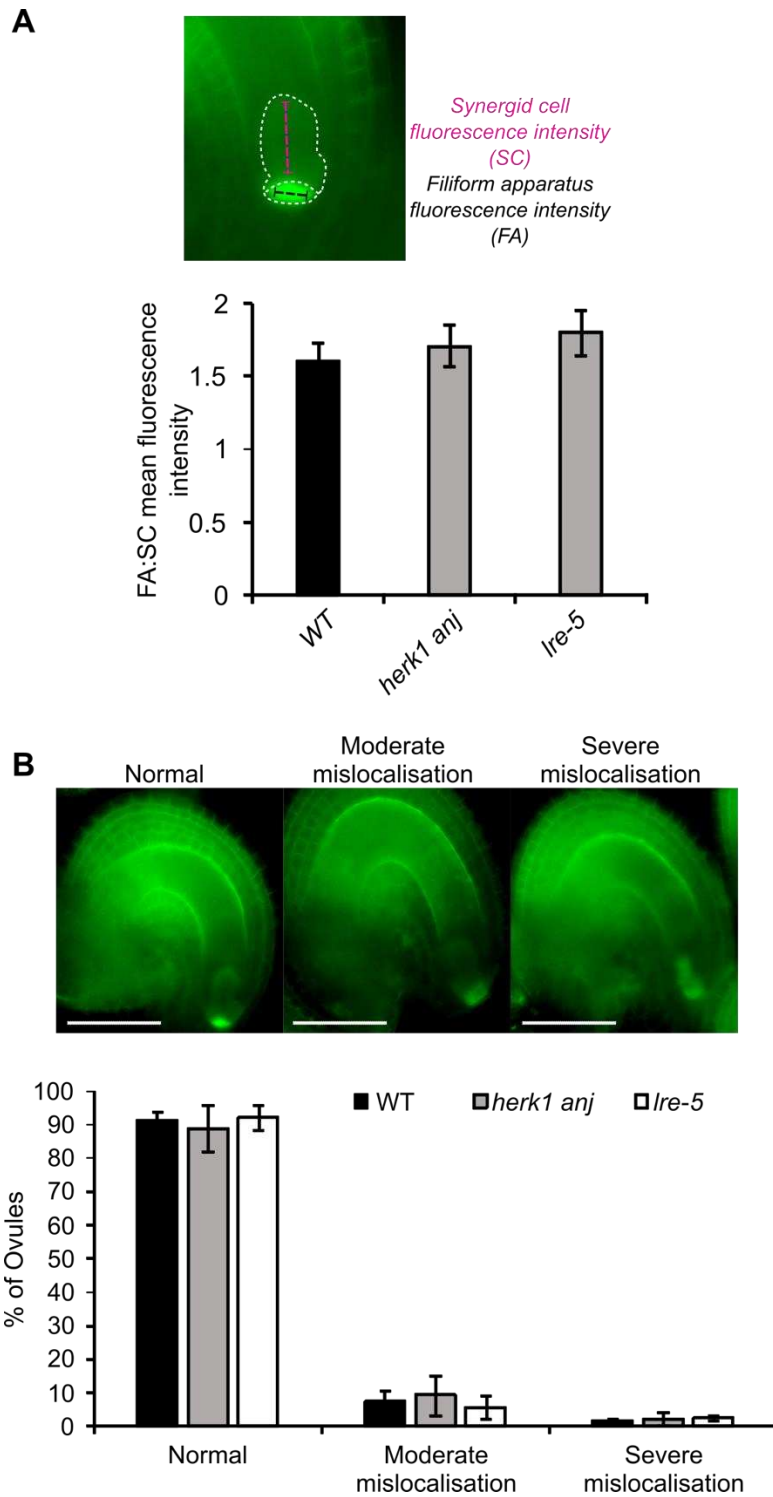
1133

1134 **Figure EV2. Kinase activity of HERK1 and ANJ is not required for complementation of the**
 1135 **pollen tube overgrowth phenotype.**

1136 A Kinase activity was assayed for wild-type HERK1, wild-type BAK1 (positive control), and kinase
 1137 dead versions (KD) of HERK1, ANJ and BAK1 using ³²P incorporation into myelin basic protein
 1138 (MyBP; trans-phosphorylation) and the cytosolic domains of the receptor kinases (CD; auto-
 1139 phosphorylation). Coomassie brilliant blue (CBB) staining of the membrane is shown below as a
 1140 loading control.

1141 B Percentage of pollen tubes displaying overgrowth at the female gametophyte in WT, *herk1 anj*
 1142 plants and at least 4 independent lines of *herk1 anj* transformed with *pHERK1::HERK1-KD* or
 1143 *pANJ::ANJ-KD-GFP* from generations T1 or T2. Pollen tube reception was scored for ovules in at
 1144 least three siliques per line ($n \geq 3$). Data presented are means \pm SD (one-way ANOVA followed by
 1145 Bonferroni's posthoc test; $p < 0.05$). *pANJ::ANJ-KD-GFP* T1 line 4 was excluded from the figure as
 1146 it likely had multiple T-DNA insertions.

1147



1149

1150 **Figure EV3. Quantification of FER-GFP mislocalisation in the synergid cells of *herk1 anj***
 1151 **and *Ire-5* ovules.**

1152 A Ratio between fluorescence intensities at the filiform apparatus (FA) and the synergid cell
 1153 cytoplasmic region (SC) in mature ovules from wild-type (Col-0), *herk1 anj* and *Ire-5* emasculated

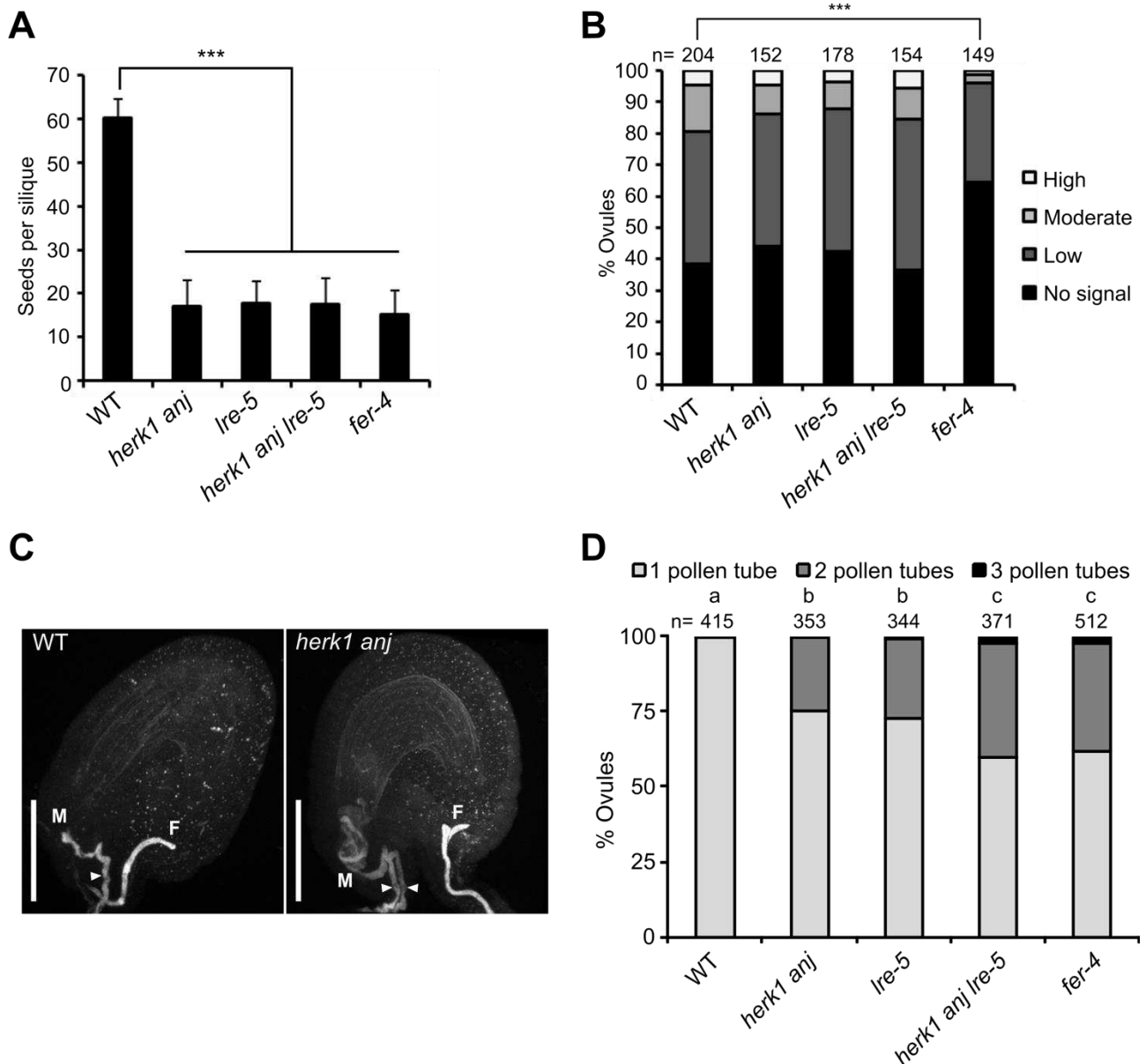
1154 flowers expressing *pFER::FER-GFP*. Fluorescence profiles for each region of the synergid cells
1155 were recorded as exemplified in the upper panel and averaged prior to the ratio calculation
1156 (Student's *t* tests, $p > 0.05$).

1157

1158 B Quantification of moderate and severe mislocalisation defects in the accumulation of FER-GFP
1159 at the filiform apparatus in mature ovules from wild-type (*Col-0*), *herk1 anj* and *lre-5* emasculated
1160 flowers expressing *pFER::FER-GFP*. Ovules with clear FER-GFP expression were assigned to
1161 one of the three categories presented in the upper panel, as per [76]. No statistically significant
1162 differences were detected in Student's *t* test comparisons with wild-type. For both analyses, at
1163 least 23 ovules obtained from three siliques per plant were scored for three plants per line, with
1164 means per plant ($n = 3$) used for the Student's *t* tests.

1165

1166



1167
 1168 **Figure EV4. HERK1, ANJ and LRE do not act additively in seed set or ROS**
 1169 **production, but mutants attract multiple pollen tubes.**

1170 A Quantification of developing seeds per silique in wild-type, *herk1 anj*, *lre-5*, *herk1 anj lre-5* and
 1171 *fer-4* plants. Fully expanded siliques were dissected and photographed under a stereomicroscope.
 1172 n = 25. Data presented are means ± SD. *** p<0.001 (Student's *t*-test).

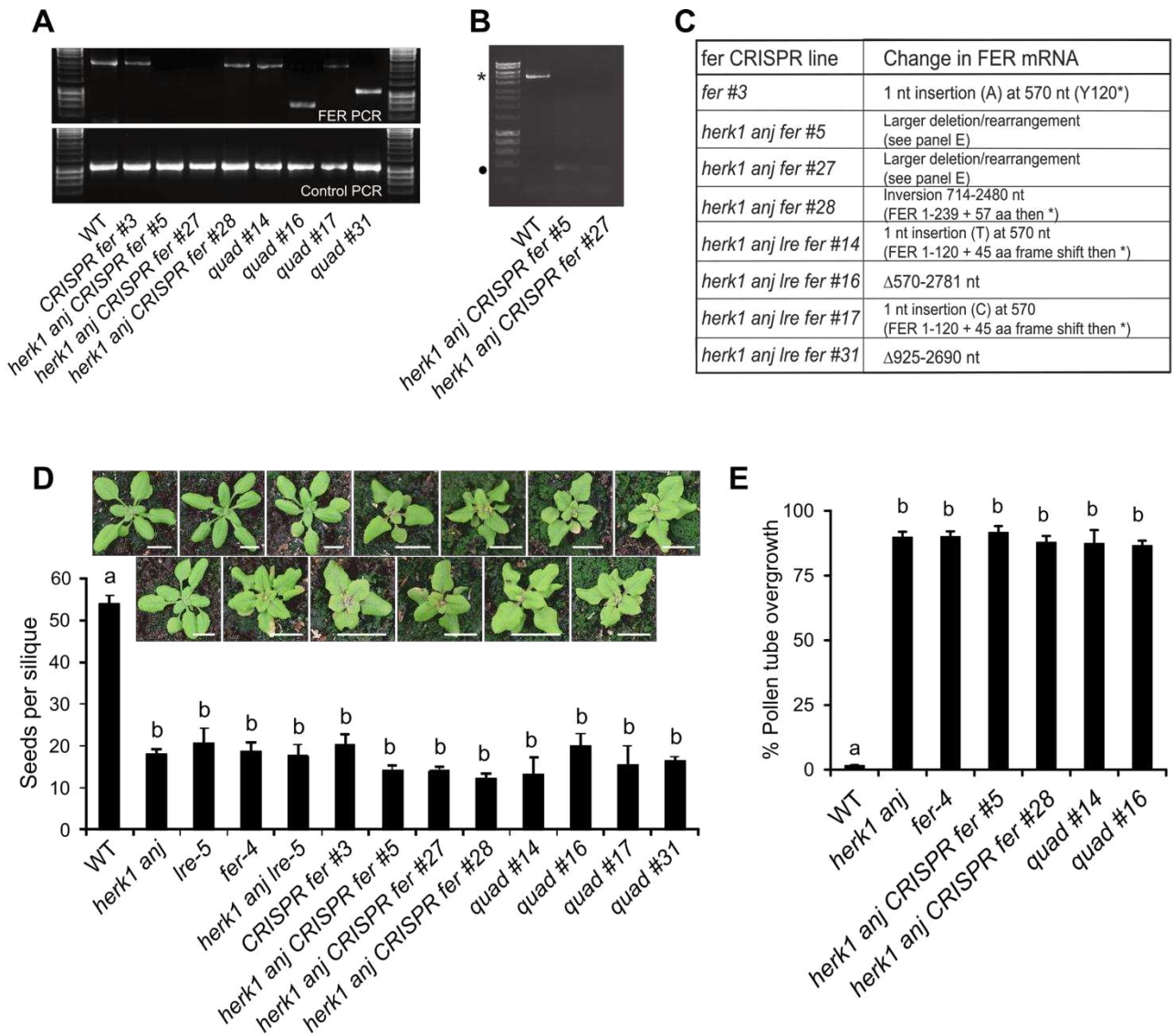
1173 B Quantification of the H₂DCF-DA staining of ROS in ovules from wild-type, *herk1 anj*, *lre-5*, *herk1*
 1174 *anj lre-5* and *fer-4* plants at 20 HAE. Categories are listed in the legend (see also Appendix Figure
 1175 S7A). Ovules dissected from at least five siliques per line. *** p<0.001 (χ -square tests).

1176 C Representative image of a normal pollen tube reception event in a wild-type ovule by confocal
1177 microscopy on the left and a *herk1 anj* ovule displaying pollen tube overgrowth and multiple pollen
1178 tubes in the micropyle on the right. Images are maximum intensity projections from confocal
1179 microscopy images across several z-planes of ovules stained with aniline blue. M, micropyle. F,
1180 funiculus. White arrowhead, pollen tube. Scale bars = 50 μ m.

1181 D Polytubey quantification in wild-type (*Col-0*), *herk1 anj*, *lre-5*, *herk1 anj lre-5* and *fer-4* ovules by
1182 epifluorescence microscopy following hand pollination at 24h after emasculation. Ovules from 10 to
1183 13 siliques per line were scored for the number of pollen tubes present at the micropyle if fertilised
1184 (total fertilised ovules analysed per line >265). Letters (a, b, c) mark statistically significant
1185 differences between samples in multiple Fisher's exact test pairwise comparisons ($p < 0.001$).

1186

1187



1188

1189

1190 **Figure EV5. Quantification of seed set in CRISPR-Cas9 *fer* mutants.**

1191 A PCR amplification of *FER* and control genomic DNA from wild-type and CRISPR-Cas9 *fer*
 1192 mutants.

1193 B For *herk1 anj CRISPR fer* lines 5 and 27, PCR of the *FER* locus using primers 1.7 kb upstream
 1194 and 1.1 kb downstream of the *CRISPR* target sites (*CRISPR-Cas9 fer* mutant genotyping outer
 1195 primers) was also performed. The expected 5.1 kb band from the wild-type Col-0 plant is indicated
 1196 by an asterisk. The band indicated by a black dot was cloned and sequenced but does not contain

1197 *FER* DNA and is therefore an artefact, leading to the conclusion that *herk1 anj CRISPR fer* lines #5
1198 and #27 contain large deletions or rearrangements that extend beyond the targeted region.

1199 C Molecular characterisation of the *CRISPR* lines.

1200 D,E Developing seeds per silique (D) and pollen tube overgrowth (E) in wild-type, single, double,
1201 triple and quadruple mutants as listed. Quad = *herk1 anj lre-5 CRISPR fer*. Fully expanded siliques
1202 were dissected and photographed using an SLR camera. Three plants per line and five siliques per
1203 plant were analysed. Data presented are means per plant ($n = 3$) \pm SD. Letters (a, b) mark
1204 statistically significant differences between samples in one-way ANOVA analysis followed by
1205 Bonferroni's post-hoc comparison of means ($p < 0.05$). Pictures above (D) are of plants at 21 days
1206 after sowing. Scale bars = 1 cm.